NPS-57VA70091A

# United States Naval Postgraduate School

AERODYNAMIC DESIGN OF SYMMETRICAL

BLADING FOR THREE-STAGE AXIAL FLOW

COMPRESSOR TEST RIG

by

M. H. Vavra

1 September 1970

NAVAL POSTGRADUATE SCHOOL

Monterey, California

Rear Admiral R. W. McNitt, USN
Superintendent

M. U. Clauser
Academic Dean

ABSTRACT:

This report deals with the aerodynamic design of an axial compressor stage with symmetrical bladings for a research program to investigate tip clearance effects in the three-stage compressor of the Turbo-Propulsion Laboratory, NPS. It establishes the blading data and the stage performance with an iterative three-dimensional approach, and gives design criteria for the drive and the flow measuring device of the test unit. The calculated distributions of the flow properties in the stage will be used for future comparisons with test data.

This task was supported by: Navy Department
Naval Air Systems Command, Code 310
AIRTASK No.
A310310A/551A/1R01003010

TABLE OF CONTENTS

LIST OF FIGURES

LIST OF TABLES

## 1. INTRODUCTION

The three-stage axial flow compressor test rig of the Turbo-Propulsion Laboratory, Department of Aeronautics, NPS, will be used to carry out a Navy sponsored research program on three-dimensional flow phenomena in compressor bladings. This compressor with a tip diameter of 36 in. and a hub/tip ratio of 0.6 is presently equipped with lightly loaded bladings which are of the free-vortex type. A 50 HP two-speed electric motor is now directly coupled to the compressor. Further details of the test rig are given in Ref. 1 (See Bibliography at end of text).

During the first phase of the research program, so-called symmetrical bladings with high aerodynamic loading will be tested. Further, in order to increase the pressure rise in the compressor, primarily to improve the measuring accuracy, the present motor will be replaced by a 150 HP motor that was obtained from surplus. This motor has the following characteristics:

Make: General Dynamics/Electro Dynamics, Bayonne, N. J.

Frame: 505 Y - Type TN

Serial No.: 70105116 A6

Cont. Load: 150 HP, 1180 rpm, 440V/3 phase, 190 Amps

It is planned also to make tests with one, two, or three stages, preferable in such a manner that the full power of the motor can be utilized in all three cases, requiring operations at different speeds. It is intended to make this possible by arranging a V-belt drive with different replaceable pulleys.

The objective of this study is to establish the aerodynamic design of the new blading, and to determine the maximum speeds at which these stages can operate at a driving power of 150 HP. These data will then be used in a future report to design the V-belt drive and the nozzle for the measuring of the compressor flow rate, since Ref. 1 shows that the presently used measuring method gives doubtful results.

The blade loadings will be such that the NASA diffusion factor does not exceed a value of 0.5 for the rotor, or 0.6 for the stator. All three stages will be identical. The flow conditions ahead of and after the blade rows will be determined with the methods of Ref. 2.

2. FIRST APPROXIMATION OF THREE-DIMENSIONAL FLOW PATTERN.

For stages with equal energy input from hub to tip without imposed radial energy gradients, the change of the axial velocity component in radial direction can be obtained from Eq. 16(50) of Ref. 2. For a first approximation it is assumed that the axial components $V_{m1}$ and $V_{m2}$ ahead of and after the rotor blades are equal at the mean radius $R_m$, and that the radial shift of the stream surfaces can be ignored. The resulting velocity diagram of the blading at the arithmetic mean radius $R_m$ is shown in Fig. 1. Figure 2 represents the conditions for a cylindrical stream surface at an arbitrary radius R between hub and tip. The actual velocity diagram for a stream surface that has the radii $R_1$ and $R_2$ ahead of and after the rotor, respectively, is given by Fig. 3. The symbols used in these figures, and in the following derivations, are defined in Ref. 2.

From Eq. 16 (42) of Ref. 2 and by Fig. 1

$$K = R \ \Delta V_u = R_m \ \Delta V_{um} = R_m \ V_m \ (\tan\beta_{1m} - \tan\beta_{2m}) \tag{1}$$

Also

$$\omega \ R_m = W_{u1m} + V_{u1m} = W_{u1m} + W_{u2m} = V_m \ (\tan\beta_{1m} + \tan\beta_{2m})$$

and

$$V_m = \frac{\omega \ R_m}{\tan\beta_{1m} + \tan\beta_{2m}} \tag{2}$$

thus

$$K = \omega \ R_m^{\ 2} \ X \tag{3}$$

where

$$X = \frac{\tan\beta_{1m} - \tan\beta_{2m}}{\tan\beta_{1m} + \tan\beta_{2m}} \tag{4}$$

From Eq. 16 (52) of Ref. 2

$$\frac{V_{u1}}{\omega R_m} = - \frac{R_m}{R} \ \frac{X}{2} + \frac{1}{2} \frac{R}{R_m} \tag{5}$$

$$\frac{V_{u2}}{\omega R_m} = + \frac{R_m}{R} \ \frac{X}{2} + \frac{1}{2} \frac{R}{R_m} \tag{6}$$

From Eq. 16 (53) of Ref. 2

$$A = - \omega R_m \frac{X}{2}; \quad B = 0; \quad C = \frac{\omega R_m}{2} \tag{7}$$

Introduced into Eq. 16 (50) of Ref. 2 for

$V_{m1} = V_{m2} = V_m$,

$$V_{a1}^2 = V_m^2 - 4AC \ln\left(\frac{R}{R_m}\right) - 2C^2 \ln \left[\left(\frac{R}{R_m}\right)^2 - 1\right] \tag{8}$$

and

$$V_{a2}^2 = V_m^2 - 4\left(A + \frac{K}{R_m}\right) C \ln\left(\frac{R}{R_m}\right) - 2C^2\left[\left(\frac{R}{R_m}\right)^2 - 1\right] \tag{9}$$

From Eqs. 8, 7 and 2

$$V_{a1}^2 = \frac{\omega^2 R_m^2}{(\tan\beta_{1m} + \tan\beta_{2m})^2} + \omega^2 R_m^2 X \ln\left(\frac{R}{R_m}\right) - \frac{\omega^2 R_m^2}{2}\left[\left(\frac{R}{R_m}\right)^2 - 1\right]$$

or

$$\left(\frac{V_{a1}}{\omega R_m}\right)^2 = Y + X \ln\left(\frac{R}{R_m}\right) - \frac{1}{2}\left[\left(\frac{R}{R_m}\right)^2 - 1\right] \tag{10}$$

where

$$Y = \frac{1}{(\tan\beta_{1m} + \tan\beta_{2m})^2} \tag{11}$$

From Eqs. 9, 7, 2, and 10

$$\left(\frac{V_{a2}}{\omega R_m}\right)^2 = Y - X \ln\left(\frac{R}{R_m}\right) - \frac{1}{2}\left[\left(\frac{R}{R_m}\right)^2 - 1\right] \tag{12}$$

Thus, the axial velocity components $V_{a1}$ and $V_{a2}$ at different radius ratios $R/R_m$ can be determined with Eqs. 11 and 12 if the angles $\beta_{1m}$ and $\beta_{2m}$ are specified at the mean radius $R_m$.

From Fig. 2

$$\tan\beta_1 = \frac{\omega R - V_{u1}}{V_{a1}} = \frac{R/R_m - V_{u1}/\omega R_m}{V_{a1}/\omega R_m}$$

With Eq. 5

$$\tan\beta_1 = \frac{\frac{R}{R_m} + \frac{R_m}{R}\,\frac{X}{2} - \frac{R}{2R_m}}{V_{a1}/\omega R_m} = \frac{\frac{R}{R_m} + \frac{R_m}{R}\,X}{2(V_{a1}/\omega R_m)} \tag{13}$$

Similarly, with Eq. 6

$$\tan\beta_2 = \frac{\omega R - V_{u2}}{V_{a2}} = \frac{\frac{R}{R_m} - \frac{R_m}{R}\,X}{2(V_{a2}/\omega R_m)} \tag{14}$$

Also from Fig. 2 and Eq. 5

$$\tan\alpha_1 = \frac{V_{u1}}{V_{a1}} = \frac{\frac{R}{R_m} - \frac{R_m}{R}\,X}{2(V_{a1}/\omega R_m)} = \tan\beta_2\,\frac{(V_{a2}/\omega R_m)}{(V_{a1}/\omega R_m)} \tag{15}$$

and with Eq. 6

$$\tan\alpha_2 = \frac{V_{u2}}{V_{a2}} = \frac{\frac{R}{R_m} + \frac{R_m}{R}\,X}{2(V_{a2}/\omega R_m)} = \tan\beta_1\,\frac{(V_{a1}/\omega R_m)}{(V_{a2}/\omega R_m)} \tag{16}$$

With these flow angles the relative and absolute velocities $W_1$, $V_2$, and $V_1$, $V_2$ are known as multiples of $\omega R_m$.

## 3. PERMISSIBLE FLOW DEFLECTIONS

The NASA diffusion factor $D_R$ of the rotor flow is defined by [Ref. 6]

$$D_R = 1 - \frac{W_2}{W_1} + \frac{\Delta W_u}{2\sigma_R W_1} \tag{17}$$

where $\sigma_R$ is the rotor solidity. The diffusion factor $D_s$ of the stator flow is

$$D_s = 1 - \frac{V_1}{V_2} + \frac{\Delta V_u}{2\,\sigma_s\,V_2} \tag{18}$$

Assuming that the stator solidity $\sigma_s$ equals $\sigma_R$, and that the chord of the stator and rotor blades does not change along the radius, there is

$$\sigma_R = \sigma_s = \sigma_m \frac{R_m}{R} \tag{19}$$

where $\sigma_m$ is the solidity at $R_m$.

From Eqs. 1 and 3

$$\Delta V_u = \Delta W_u = \frac{K}{R} = \omega R_m \frac{R_m}{R} X \tag{20}$$

Then from Eq. 17 with 19

$$D_R = 1 - \frac{V_{a2}/\omega R_m}{V_{a1}/\omega R_m} \frac{\cos\beta_1}{\cos\beta_2} + \frac{X \cos\beta_1}{2\,\sigma_m (V_{a1}/\omega R_m)} \tag{21}$$

Also by Eqs. 18, 19, and 20

$$D_s = 1 - \frac{V_{a1}/\omega R_m}{V_{a2}/\omega R_m} \frac{\cos\alpha_2}{\cos\alpha_1} + \frac{X \cos\alpha_2}{2\,\sigma_m (V_{a2}/\omega R_m)} \tag{22}$$

For the chosen conditions the diffusion factors $D_R$ and $D_s$ at the mean radius $R_m$ are equal, say, equal to $D_m$, where by Eqs. 21, 2, and 4

$$D_m = 1 - \frac{\cos\beta_{1m}}{\cos\beta_{2m}} + \frac{(\tan\beta_{1m} - \tan\beta_{2m}) \cos\beta_{1m}}{2\,\sigma_m} \tag{23}$$

Equation 23 can be rearranged to calculate directly the flow angle $\beta_{2m}$ for specified values of $\beta_{1m}$, $D_m$, and $\sigma_m$. Equation 23 rewritten

$$\frac{1 - D_m}{\cos\beta_{1m}} = \frac{1}{\cos\beta_{2m}} - \frac{\tan\beta_{1m}}{2\sigma_m} + \frac{\tan\beta_{2m}}{2\sigma_m}$$

Hence

$$\tan\beta_{1m} + \frac{2\sigma_m(1 - D_m)}{\cos\beta_{1m}} = \tan\beta_{2m} + \frac{2\sigma_m}{\cos\beta_{2m}}$$

Let

$$E = \tan\beta_{1m} + \frac{2\sigma_m(1 - D_m)}{\cos\beta_{1m}} \tag{24}$$

then

$$E = \frac{\sin\beta_{2m} + 2\sigma_m}{\cos\beta_{2m}} = \frac{\sin\beta_{2m} + 2\sigma_m}{\sqrt{1 - \sin^2\beta_{2m}}}$$

and

$$\sin\beta_{2m} = \frac{-2\sigma_m \overset{+}{(-)} E\sqrt{1 + E^2 - 4\sigma_m 2}}{1 + E^2} \tag{25}$$

It is possible also to determine the deflection angle

$$\Delta\beta = \beta_{1m} - \beta_{2m} \tag{26}$$

from Eq. 23. This relation rearranged

$$2\sigma_m \cos\beta_{2m}(1 - D_m) = 2\sigma_m \cos\beta_{1m} - (\tan\beta_{1m} - \tan\beta_{2m})\cos\beta_{1m}\cos\beta_{2m}$$

$$= 2\sigma_m \cos\beta_{1m} - (\sin\beta_{1m} \cos\beta_{2m} - \cos\beta_{1m} \sin\beta_{2m})$$

$$= 2\sigma_m \cos\beta_{1m} - \sin(\beta_{1m} - \beta_{2m})$$

$$= 2\sigma_m \cos\beta_{1m} - \sin \Delta\beta$$

Since from Eq. 26

$$\beta_{2m} = \beta_{1m} - \Delta\beta$$

there is

$$2\sigma_m(1 - D_m)(\cos\beta_{1m}\cos\Delta\beta + \sin\beta_{1m}\sin\Delta\beta) = 2\sigma_m \cos\beta_{1m} - \sin\Delta\beta$$

and

$$\sin\Delta\beta \left[ \tan\beta_{1m} + \frac{1}{2\sigma_m(1-D_m)\cos\beta_{1m}} \right] = \frac{1}{1 - D_m} + \cos\Delta\beta$$

with

$$F = \tan\beta_{1m} + \frac{1}{2\sigma_m \ (1-D_m)\cos\beta_{1m}} \tag{27}$$

there is

$$\sin\Delta\beta = \frac{F \underset{(+)}{-} \sqrt{(1-D_m)^2 \ (1+F^2) \ -1}}{(1-D_m) \ (1+F^2)} \tag{28}$$

For chosen values $\beta_{1m}$, $\sigma_m$, and $D_m$ the flow angles $\beta_{2m}$ can therefore be determined. The angles $\beta_{1m}$ and $\beta_{2m}$ then establish the quantities X and Y of Eqs. 4 and 11, respectively. Introduced into Eqs. 10 and 12 these values can be used to obtain the changes of the axial components $V_{a1}$ and $V_{a2}$ in radial direction. With the angles $\beta_1$ and $\beta_2$ from Eqs. 13 and 14 it is then possible to calculate the diffusion factors $D_R$ and $D_s$ at particular radii with Eqs. 21 and 22.

## 4. APPROXIMATE OPERATING CONDITIONS OF COMPRESSOR.

The following relations will be used to establish the main parameters of the blading, which later on will be investigated in more detail.

If it is assumed that $V_m$ is equal to the average through-flow velocity in the compressor annulus, the volume flow rate Q is

$$Q = A_c V_m$$

where $A_c$ is the cross-sectional area of the annulus. With Eq. 2

$$Q = A_c \ \omega R_m \ \frac{1}{\tan\beta_{1m} + \tan\beta_{2m}} \quad [\mathrm{ft}^3/\mathrm{sec}] \tag{29}$$

The driving moment M for one stage is

$$\dot{M} = \mathring{m} R_m \Delta V_u = \mathring{m} K \qquad [\text{ft-lb}] \tag{30}$$

Because of the small pressure rise in the compressor the mass flow rate $\mathring{m}$ can be taken as

$$\mathring{m} = Q \rho_o \tag{31}$$

where $\rho_o$ is the air density at ambient conditions. For z stages (z = 1, 2, or 3) the necessary horsepower HP is

$$HP = z \frac{\omega M}{550} = z \frac{\rho_o \omega^3 R_m^3 A_c (\tan\beta_{1m} - \tan\beta_{2m})}{550} \tag{32}$$

At 14.7 psia and 60°F

$$\rho_o = 2.371 \, (10^{-3}) \qquad [\text{slug/ft}^3]$$

With the rotational speed N in rpm

$$\omega = \frac{\pi N}{30}$$

For a tip diameter of 3 feet and a hub/tip ratio of 0.6

$$A_c = \frac{\pi}{4} 3^2 (1 - 0.6^2) = 4.524 \text{ ft}^2$$

$$R_m = 1.5 \frac{(1 + 0.6)}{2} = 1.2 \text{ ft}$$

Then, from Eq. 29

$$Q = \frac{(0.568) \, N}{\tan\beta_{1m} + \tan\beta_{2m}} \qquad [\text{ft}^3/\text{sec}] \tag{33}$$

From Eq. 30

$$HP = (38.7) z \left( \frac{N}{1000} \right)^3 (\tan\beta_{1m} - \tan\beta_{2m}) \tag{34}$$

Assuming that 135 HP are absorbed at the design point, to have available 150 HP at overload conditions, the design operating speed is obtained from

$$N = \frac{1516.6}{\left[ z \, (\tan\beta_{1m} - \tan\beta_{2m}) \right]^{\frac{1}{3}}} \qquad [\text{rpm}] \tag{35}$$

If $\Delta P_t$ is the rise of the total pressure in the stage, and $\eta$ the total-to-total stage efficiency, there is

$$\frac{Q\ \Delta P_t}{\eta} = M\omega = HP(550) \tag{36}$$

With Eqs. 30, 31 and 3

$$\frac{\Delta P_t}{\eta} = \frac{M\omega}{Q} = \rho_\circ K\omega = \rho_\circ \omega^2 R_m^{\ 2} X \tag{37}$$

For a driving power of 135 HP, the pressure rise $\Delta P_t$ is obtained directly from the second equality of Eq. 36. With Eq. 33,

$$\frac{\Delta P_t}{\eta} = 130.72 \ \frac{\tan\beta_{1m} + \tan\beta_{2m}}{(N/1000)} \quad [lb/ft^2]$$

or

$$\frac{\Delta P_t}{\eta} = 25.14 \ \frac{\tan\beta_{1m} + \tan\beta_{2m}}{(N/1000)} \quad [in.H_2O] \tag{38}$$

## 5. DETERMINATION OF BLADING PARAMETERS.

Most desirable for the present tests are bladings that produce the highest pressure rise at the lowest speed of rotation. Such bladings will also have low flow rates. Figures 4 and 5 show that the angles $\beta_{1m}$ should be as high as possible for these conditions. Figure 6 indicates that the speed of rotation is not changing greatly with $\beta_{1m}$ and that its magnitude is primarily a function of the diffusion factor $D_m$, which should be as high as possible.

Figure 7 shows the flow deflections $\Delta\beta = \beta_{1m} - \beta_{2m}$ for different angles $\beta_{1m}$ and diffusion factors $D_m$ at a solidity $\sigma_m = 1$, which establish the quantities X and Y of Eqs. 4 and 11, respectively. These values introduced into Eq. 12 show that the axial velocity $V_{a2}$ becomes imaginary for $\beta_{1m}$ greater than a particular angle $\beta_{1m}{}^*$ which is depending on $D_m$. These limits of $\beta_{1m}{}^*$ for $V_{a2} = 0$ are:

$D_m$ = 0.30 0.35 0.40 0.45

$\beta_{1m}^*$ = 45.7° 47.2° 47.8° 48.4°

Hence the flow angles $\beta_{1m}$ cannot exceed about 45°.

Table I gives the flow conditions along the radius for $\beta_{1m}$ = 45° and $D_m$ = 0.4 at the mean radius $R_m$, as calculated by the previously established relations. It can be noted that the diffusion factor $D_R$ at the rotor tip is in excess of 0.56, hence unacceptably high. For $\beta_{1m}$ = 45° and $D_m$ = 0.35 the resulting data are listed in Table II. Although $D_R$ at the rotor tip is about 0.5, the large deceleration of the axial velocity components at the outer radius from $V_{a1}/\omega R_m$ = 0.4445 to $V_{a2}/\omega R_m$ = 0.2629, together with the negative flow deflection $\Delta\beta$ at this station, make this blading undesirable for the present purposes. The angle $\beta_{1m}$ is therefore taken as 40° and Table III lists the data obtained for $D_m$ = 0.4. For this value the diffusion factor $D_R$ at the rotor tip is larger than 0.5. Repeating the calculations for $\beta_{1m}$ = 40° and $D_m$ = 0.35 gave the flow conditions of Table IV which seem acceptable in all respects. These parameters are therefore chosen for a more detailed investigation of the flow conditions by taking account of the radial shift of the stream surfaces from rotor inlet to rotor discharge with the resulting velocity diagram of Fig. 3.

6. METHOD FOR BETTER APPROXIMATION OF FLOW CONDITIONS.

The quantities listed in Table IV will be called the first approximation of the flow conditions. Figure 8 shows the velocity ratios $V_{a1}/(\omega R_m)$ and $V_{a2}/(\omega R_m)$ of this approximation as functions of the radius ratio $R/R_m$. These values were obtained by assuming that $V_{a1}$ and $V_{a2}$ at $R_m$ are equal, and identical with the quantity $V_m$ of Eqs. 8 and 9. Moreover a fluid particle entering the rotor at a radius $R_1$ is supposed to leave the rotor at the same radius, or $R_2 = R_1 = R$. This condition led to Eq. 1 which formulates that all fluid particles receive the same energy increase $\Delta H$ in the rotor. However if $R_1$ and $R_2$ differ, this requirement must be expressed by

$$\Delta H = \omega(R_2\, V_{u2} - R_1\, V_{u1}) = \text{Constant} \tag{39}$$

If it is assumed that the energy increase $\Delta H$ in the stage is that of the first approximation, there is from Eqs. 1 and 3

$$\Delta H = \omega K = \omega^2 R_m^{\ 2} X \qquad (40)$$

where, from Table IV,

$$X = 0.36578$$

Now, if the tangential components $V_{u1}$ along the radius $R_1$ ahead of the rotor are taken to be those of the first approximation, namely, by Eq. 5

$$\frac{V_{u1}}{\omega R_m} = -\frac{R_m}{R_1}\frac{X}{2} + \frac{1}{2}\frac{R_1}{R_m} \qquad (41)$$

the distribution of $V_{u2}$ along the radius $R_2$ after the rotor is from Eqs. 39, 40 and 41,

$$\frac{V_{u2}}{\omega R} = \frac{R_m}{R_2}\left[\frac{X}{2} + \frac{1}{2}\left(\frac{R_1}{R_m}\right)^2\right] \qquad (42)$$

Thus, to satisfy Eq. 39, the components $V_{u2}$ can be determined only if the corresponding radii $R_1$ and $R_2$ of the stream surfaces are known. The results of the first approximation will be used to establish an approximate relationship between $R_1$ and $R_2$ by applying the equation of continuity. In particular, for a chosen value of $R_1$ the corresponding radius $R_2$ is found from the condition that the same mass flow rate has to occur between $R_2$ and the hub radius $R_{2h}$, as between the radius $R_1$ and the hub radius $R_{1h}$. The adopted procedure is explained in the next paragraph. With $R_2$ known as a function of $R_1$, the distribution of the components $V_{u2}$ in radial direction are obtained from Eq. 42. The axial components $V_{a2}$ along $R_2$ can then be determined by solving Eq. 16 (41) of Ref. 2, or

$$\frac{\partial (V_{a2})^2}{\partial R_2} = -\frac{2\,V_{u2}}{R_2}\frac{\partial (R_2 V_{u2})}{\partial R_2} \qquad (43)$$

if the curvatures of the generatrices of the stream surfaces and radial entropy gradients are ignored. The data obtained in this manner from Eq. 43 represent the so-called second approximation. Applied to the equation of continuity they permit a check of the relationship between $R_1$ and $R_2$. If this interdependence does not correspond to that obtained from the first approximation, it will be necessary to carry out further iterations.

Evidently, if curvature effects and entropy gradients are ignored, the distribution of $V_{a1}$ along $R_1$ for $V_{u1}$ of Eq. 41 is not affected by the radial shift from $R_1$ and $R_2$, hence the flow conditions ahead of the rotor are those given in Table IV.

The relations for the second and, if necessary, further approximations, can be simplified by introducing the following dimensionless quantities:

$$
\begin{aligned}
r_1 &= \frac{R_1}{R_m} \quad ; & r_2 &= \frac{R_2}{R_m} \\
V_{a1}^* &= \frac{V_{a1}}{\omega R_m} \quad ; & V_{a2}^* &= \frac{V_{a2}}{\omega R_m} \\
V_{u1}^* &= \frac{V_{u1}}{\omega R_m} \quad ; & V_{u2}^* &= \frac{V_{u2}}{\omega R_m} \\
V_{m1}^* &= \frac{V_{m1}}{\omega R_m} \quad ; & V_{m2} &= \frac{V_{m2}}{\omega R_m}
\end{aligned}
\tag{44}
$$

Then, Eq. 42 rewritten is

$$V_{u2}^* = \frac{1}{2r_2} \left( X + r_1^2 \right) \tag{45}$$

and Eq. 43 becomes

$$\frac{\partial \left( V_{a2}^* \right)^2}{\partial r_2} = - \left[ \frac{X}{r_2^2} + \left( \frac{r_1}{r_2} \right)^2 \right] \frac{1}{2} \, \frac{\partial (X + r_1^2)}{\partial r_2}$$

Since X is a constant,

$$\frac{\partial\left(V_{a2}^{*}\right)^{2}}{\partial r_2} = -\left[\frac{X + r_1^{2}}{r_2^{2}}\right] r_1 \frac{\partial r_1}{\partial r_2} = -f(r_2) \qquad (46)$$

Hence, if $r_1$ is known as a function of $r_2$, the function $f(r_2)$ can be established. Denoting the as yet unknown value of $V_{a2}^{*}$ at $r_2 = 1$ by $V_{m2}^{*}$, the integration of Eq. 46 gives

$$\left(V_{a2}^{*}\right)^{2} = \left(V_{m2}^{*}\right)^{2} - \int_{1}^{r_2} f(r_2)\, dr_2 \qquad (47)$$

The quantity $V_{m2}^{*}$ must be obtained by iterations with the help of the equation of continuity. Figure 4 shows that the pressure rise per stage does not exceed 16 inches of water. In a stage with 50 percent reaction the pressure rise in the rotor is then about 8 inches of water, giving a pressure ratio of about 1.02 for an inlet pressure of 14.7 psia. The ratio $\rho_2/\rho_1$ of the mass density after and ahead of the rotor will therefore not exceed a value of 1.014.

The volume flow rate $Q_1$ ahead of the rotor between the hub radius $R_{1h}$ and an arbitrary radius $R_1$ is

$$Q_1 = 2\pi \int_{R_{1h}}^{R_1} R_1 V_{a1}\, dR_1$$

With the quantities of Eq. 44 let

$$Q_1 = 2\pi\omega R_m^{3} Q_1^{*} \qquad (48)$$

by introducing the dimensionless quantity

$$Q_1^{*} = \int_{R_{1h}/R_m}^{r_1} r_1 Va_1^{*}\, dr_1 \qquad (49)$$

The total volume flow rate $Q_{1max}$ ahead of the rotor is

$$Q_{1max} = 2\pi\omega R_m^{3} Q_{1max}^{*} \qquad (50)$$

where $Q^*_{1max}$ is obtained from Eq. 49 for the upper limit $r_1 = R_{1t}/R_m$ of the integral, where $R_{1t}$ is the tip radius.

Similarly, for the conditions after the rotor the volume flow rate $Q_2$ between $R_{2h}$ and $R_2$ is

$$Q_2 = 2\pi\omega R_m^3 \; Q_2^* \tag{51}$$

$$\text{with} \quad Q_2^* = \int_{R_{2h}/R_m}^{r_2} r_2 \, V_{a2}^* \, dr_2 \tag{52}$$

The total volume flow rate $Q_{2max}$ at station 2 is

$$Q_{2max} = 2\pi\omega \, R_m^3 \; Q^*_{2max} \tag{53}$$

The quantity $Q^*_{2max}$ is obtained from Eq. 52 for the upper limit $r_2 = R_{2t}/R_m$ of the integral.

The equality of the mass flow rates at stations (1) and (2) can be expressed by

$$\bar{\rho}_1 \, Q_{max} = \bar{\rho}_2 \, Q_{2max} \, k_B'$$

where $\bar{\rho}_1$, $\bar{\rho}_2$ are the average mass densities at (1) and (2), and $k_B'$ is the so-called blockage factor that takes account of the increased regions of reduced velocity in the so-called wall boundary layers near the hub and the tip at station (2), compared to those at station (1). Then, with Eqs. 50 and 53

$$Q^*_{2max} = \frac{Q^*_{1max}}{(\bar{\rho}_2/\bar{\rho}_1)k_B'} = \frac{Q^*_{1max}}{k_B} \tag{54}$$

Experience shows that the blockage factor $k_B'$ varies between 0.96 and 0.97. Hence, since $\bar{\rho}_2/\bar{\rho}_1 \cong 1.014$, the quantity $Q^*_{2max}$ will be determined by Eq. 54 with a factor $k_B = (1.014)(0.965) = 0.98$ for the value of $Q^*_{1max}$ obtained from Eq. 49. This value of $Q^*_{2max}$ is used to

$$\frac{\partial\left(V_{a2}^{*}\right)^{2}}{\partial r_2} = -\left[\frac{X + r_1^{2}}{r_2^{2}}\right] r_1 \frac{\partial r_1}{\partial r_2} = -f(r_2) \tag{46}$$

Hence, if $r_1$ is known as a function of $r_2$, the function $f(r_2)$ can be established. Denoting the as yet unknown value of $V_{a2}^{*}$ at $r_2 = 1$ by $V_{m2}^{*}$, the integration of Eq. 46 gives

$$\left(V_{a2}^{*}\right)^{2} = \left(V_{m2}^{*}\right)^{2} - \int_{1}^{r_2} f(r_2)\, dr_2 \tag{47}$$

The quantity $V_{m2}^{*}$ must be obtained by iterations with the help of the equation of continuity. Figure 4 shows that the pressure rise per stage does not exceed 16 inches of water. In a stage with 50 percent reaction the pressure rise in the rotor is then about 8 inches of water, giving a pressure ratio of about 1.02 for an inlet pressure of 14.7 psia. The ratio $\rho_2/\rho_1$ of the mass density after and ahead of the rotor will therefore not exceed a value of 1.014.

The volume flow rate $Q_1$ ahead of the rotor between the hub radius $R_{1h}$ and an arbitrary radius $R_1$ is

$$Q_1 = 2\pi \int_{R_{1h}}^{R_1} R_1 V_{a1}\, dR_1$$

With the quantities of Eq. 44 let

$$Q_1 = 2\pi\omega\, R_m^{3}\, Q_1^{*} \tag{48}$$

by introducing the dimensionless quantity

$$Q_1^{*} = \int_{R_{1h}/R_m}^{r_1} r_1\, Va_1^{*}\, dr_1 \tag{49}$$

The total volume flow rate $Q_{1max}$ ahead of the rotor is

$$Q_{1max} = 2\pi\omega\, R_m^{3}\, Q_{1max}^{*} \tag{50}$$

where $Q^*_{1max}$ is obtained from Eq. 49 for the upper limit $r_1 = R_{1t}/R_m$ of the integral, where $R_{1t}$ is the tip radius.

Similarly, for the conditions after the rotor the volume flow rate $Q_2$ between $R_{2h}$ and $R_2$ is

$$Q_2 = 2\pi\omega R_m^3 \; Q_2^* \tag{51}$$

$$\text{with} \quad Q_2^* = \int_{R_{2h}/R_m}^{r_2} r_2 \; V_{a2}^* \; dr_2 \tag{52}$$

The total volume flow rate $Q_{2max}$ at station 2 is

$$Q_{2max} = 2\pi\omega \; R_m^3 \; Q^*_{2max} \tag{53}$$

The quantity $Q^*_{2max}$ is obtained from Eq. 52 for the upper limit $r_2 = R_{2t}/R_m$ of the integral.

The equality of the mass flow rates at stations (1) and (2) can be expressed by

$$\bar{\rho}_1 \; Q_{max} = \bar{\rho}_2 \; Q_{2max} \; k_B'$$

where $\bar{\rho}_1$, $\bar{\rho}_2$ are the average mass densities at (1) and (2), and $k_B'$ is the so-called blockage factor that takes account of the increased regions of reduced velocity in the so-called wall boundary layers near the hub and the tip at station (2), compared to those at station (1). Then, with Eqs. 50 and 53

$$Q^*_{2max} = \frac{Q^*_{1max}}{(\bar{\rho}_2/\bar{\rho}_1)k_B'} = \frac{Q^*_{1max}}{k_B} \tag{54}$$

Experience shows that the blockage factor $k_B'$ varies between 0.96 and 0.97. Hence, since $\bar{\rho}_2/\bar{\rho}_1 \cong 1.014$, the quantity $Q^*_{2max}$ will be determined by Eq. 54 with a factor $k_B = (1.014)(0.965) = 0.98$ for the value of $Q^*_{1max}$ obtained from Eq. 49. This value of $Q^*_{2max}$ is used to check whether the distribution of $V_{a2}^*$ along $r_2$, obtained from Eq. 47 with a chosen value of $V_{m2}^*$, meets the continuity requirements. To this end the ratios $V_{a2}^*$, thus determined, are introduced into Eq. 52 and integrated from $R_{2h}/R_m$ to $R_{2t}/R_m$. If the resulting quantity $Q_{2max}^*$ differs from $Q_{1max}^*/k_B$ of Eq. 54, the process must be repeated with a new value of $V_{m2}^*$ until agreement is reached. However, the final distribution of $V_{a2}^*$ along $r_2$ must also produce the same radial shift of the streamlines as was determined from the first approximation, and which was used to establish the function $f(r_2)$ of Eq. 46 and $V_{a2}^*$ by Eq. 47. The equation of continuity is again used to obtain $r_2$ as function of $r_1$ from the new $V_{a2}^*$ - distribution. If this relationship between $r_2$ and $r_1$ differs from the one obtained with the data of the first approximation, it must be used to establish a new function $f(r_2)$ of Eq. 46 which has to be introduced into Eq. 47 to calculate $V_{a2}^*$. This process requires the same iterations for $V_{m2}^*$ as discussed above. The iterative procedure must be repeated until the functions $r_2$ vs. $r_1$ assumed for the determination of $f(r_2)$ and that obtained from the resulting profile of $V_{a2}^*$ are identical.

## 7. RESULTS OF FLOW CALCULATIONS

Table V lists the ratios $V_{a1}^*$ and $V_{a2}^*$ of Table IV, and additional values at other radius ratios, which were used to calculate the quantities $Q_1^*$ and $Q_2^*$ in accordance with Eqs. 49 and 52, by integrations with the trapezoidal rule. It can be noted that the initial assumption $V_{m1} = V_{m2} = V_m$ does not satisfy continuity since $Q_{2max}^*$ is $(0.9832)Q_{1max}^*$, whereas by Eq. 54 with $k_B = 0.98$ it should be (1.0204) $Q_{1max}^*$, or equal to 0.404947.

The ratios $Q_1/Q_{1max}$, and $Q_2/Q_{2max}$ of Table V are plotted in Fig. 9. For the condition $Q_2/Q_{2max} = Q_1/Q_{1max}$, the radius ratio $r_2$ for a stream surface that has the radius ratio $r_1$ ahead of the rotor can be read on the upper horizontal scale of the figure. The relationship $r_1$ vs. $r_2$ thus obtained is shown in Fig. 10, which also gives a curve $\Delta r = (r_1 - r_2)$ as function of $r_2$ in a larger scale drawn through the data points. From this curve were obtained the derivatives $\partial(\Delta r)/\partial r_2$ by graphical means. Then

$$\frac{\partial r_1}{\partial r_2} = \frac{\partial(r_2 + \Delta r)}{\partial r_2} = 1 + \frac{\partial(\Delta r)}{\partial r_2} \tag{55}$$

The numerical values of these derivatives and of $r_1$ for different ratios $r_2$ are listed in Table VI, together with the function $f(r_2)$ of Eq. 46 for X = 0.36578.

The function $f(r_2)$ is plotted in Fig. 11. Interpolated values between the calculated points were used to integrate $f(r_2)$ with Simpson's rule, i.e. by placing a parabola through three neighboring points. The results of the integration in accordance with Eq. 47 are listed in Table VI and plotted in Fig. 11. Table VI also shows the calculated values of $V_{a2}^*$ in accordance with Eq. 47, for several assumed values of $V_{m2}^*$, and the corresponding magnitudes of $Q_2^*$ of Eq. 52 obtained by integrations with the trapezoidal rule. As pointed out earlier, the value of $Q_2^*$ at $r_2$ = 1.25, which is denoted by $Q_{2max}^*$, should equal 0.404947. For $V_{m2}^*$ = 0.838 this condition is closely realized and the corresponding values of $V_{a2}^*$ are taken to satisfy the continuity requirement. For $V_{m2}^*$ = 0.838 the ratios $Q_2/Q_{2max}$ are shown in Table VI also.

It must now be checked whether the relation between $r_1$ and $r_2$ from the first approximation of Fig. 9, which was used to calculate the velocity distributions of Table VI, agrees with the function $r_2$ vs. $r_1$ that is obtained from the second approximation. Since the change of $V_{u1}^*$ along $r_1$, hence of $V_{a1}^*$ along $r_1$, is the same for both approximations, this check can be made by plotting $Q_2/Q_{2max}$ as function of $r_2$ for both sets of data. Figure 12 shows a curve of $Q_2/Q_{2max}$ vs. $r_2$ drawn through the values of Fig. 9 which are marked by crosses. The data points given by circles in Fig. 12 represent the values of Table VI for $V_{m2}^*$ = 0.838. It can be noted that these points lie very closely on the curve of the first approximation, hence additional iterations are unnecessary, and the data inside the heavily framed portion of Table VI can be considered to represent the actual flow conditions after the rotor for the set of initial assumptions; that is, if curvature effects and entropy gradients are ignored. This final distribution of $V_{a2}^*$ is also shown by the dash-dotted curve in Fig. 8.

Table VII summarizes the flow properties ahead of and after the rotor in accordance with the data of Table VI. Since the velocity diagram of the blading is that of Fig. 3, there are, with Eq. 41

$$V_{u1}^{*} = \frac{V_{u1}}{\omega R_m} = -\frac{X}{2r_1} + \frac{r_1}{2} \tag{56}$$

and

$$W_{u1}^{*} = \frac{W_{u1}}{\omega R_m} = \frac{\omega R_1 - V_{u1}}{\omega R_m} = r_1 - V_{u1}^{*} = \frac{X}{2r_1} + \frac{r_1}{2} \tag{57}$$

Thus

$$\tan\alpha_1 = \frac{V_{u1}^{*}}{V_{a1}^{*}} \tag{58}$$

and

$$\tan\beta_1 = \frac{W_{u1}^{*}}{V_{a1}^{*}} \tag{59}$$

With Eq. 45 and from Fig. 3

$$W_{u2}^{*} = \frac{W_{u2}}{\omega R_m} = \frac{\omega R_2 - V_{u2}}{\omega R_m} = r_2 - V_{u2}^{*} \tag{60}$$

and

$$\tan\alpha_2 = \frac{V_{u2}^{*}}{V_{a2}^{*}} \tag{61}$$

$$\tan\beta_2 = \frac{W_{u2}^{*}}{V_{a2}^{*}} \tag{62}$$

Also

$$V_1^{*} = \frac{V_1}{\omega R_m} = \frac{V_{a1}^{*}}{\cos\alpha_1} \tag{63}$$

$$W_1^{*} = \frac{W_1}{\omega R_m} = \frac{V_{a1}^{*}}{\cos\beta_1} \tag{64}$$

$$V_2^* = \frac{V_2}{\omega R_m} = \frac{V_{a2}^*}{\cos\alpha_2} \tag{65}$$

$$W_2^* = \frac{W_2}{\omega R_m} = \frac{V_{a2}^*}{\cos\beta_2} \tag{66}$$

Table VII also lists the NASA diffusion factors of Eqs. 17 and 18, where the subscripts o in $(D_R)_o$ and $(D_S)_o$ indicate that these factors are for a solidity $\sigma = \sigma_m = 1$ at $R/R_m = 1$, and that the chord of the rotor and stator blades does not change in radial direction. In actuality the diffusion factors should be calculated for the conditions along the stream surfaces by taking account of their radial shift. Then, by Ref. 3, for the rotor

$$D_R = 1 - \frac{W_2}{W_1} + \frac{R_1 W_{u1} - R_2 W_{u2}}{\sigma_R (R_1 + R_2) W_1} \tag{67}$$

A similar expression is defined in Ref. 3 for stators. However, in the present case where the radial shift is slight, the relations of Eqs. 17 and 18 can be used with very small error. In fact, the differences are so insignificant that the blade profiles in stator and rotor will be determined for cylindrical stream surfaces, with the actual flow angles of Table VII, instead of along the actual stream surfaces. This procedure avoids the difficulties associated with the definition of the blade shapes for manufacturing purposes. If the profiles are considered to lie on arbitrary stream surfaces, the resulting blade shapes must later be intersected by cylinders, or by planes tangent to them, to be able to obtain profile coordinates that can be used and checked during manufacture with reasonable cost. The available calculating methods for the profile shapes and their angular orientation are not accurate enough to warrant the difficulties associated with the afore-mentioned procedure, particularly not because the theoretical, axisymmetric,stream surfaces are very nearly cylindrical in the present case. It must also be recognized that the actual stream surfaces in a blade row are not axisymmetric, hence particles that move along the two sides of a blade travel along different paths with different radii so that the flow does not have the same two-dimensional character that exists in rectilinear cascade test rigs which were used to establish the profile design data.

In addition to, or as a replacement of the diffusion factor, the so-called equivalent diffusion ratio $D_{EQ}$ is frequently used to establish the blade loading limits and the profile losses, especially if the flow incidence angles differ from those for minimum losses. By Ref. 4, for rotors at the design incidence angle, and for flows with varying through-flow components on cylindrical stream surfaces,

$$D_{EQR} = \frac{W_1}{W_2} \left[ 1.12 + \frac{0.61}{\sigma_R} \cos^2\beta_1 \frac{2\Delta W_u}{V_{a1} + V_{a2}} \right] \tag{68}$$

For stators at the same conditions,

$$D_{EQS} = \frac{V_2}{V_1} \left[ 1.12 + \frac{0.61}{\sigma_S} \cos^2\alpha_2 \frac{2\Delta V_u}{V_{a1} + V_{a2}} \right] \tag{69}$$

Experience has shown that the quantities $D_{EQ}$ should not exceed values of about 1.7 since incipient flow separation is likely to occur for $D_{EQ}$ between 2.0 and 2.2. The subscripts o in $(D_{EQR})_o$ and $(D_{EQS})_o$ of Table VII indicate that $\sigma_R = \sigma_S = 1$ at the mean radius $R_m$ and that the blades have constant chord at all radii.

## 8. BLADE PROFILES AND STAGGER ANGLES

The thickness distribution of Fig. 13 will be used for the profiles of the stator and rotor blades. It corresponds to a C.4 base profile (See Ref. 5), except for the portions near the entrance which were thinned to arrange a smaller leading edge radius. The camber line of the profile is supposed to be a circular arc. Figure 14 shows the method that will be adopted to determine the profile coordinates for known camber angles $\alpha$ and maximum thickness ratios t/c. The orientation of the blade profiles in the cascade is fixed by the stagger angle $\gamma$ as indicated in Fig. 14.

The profile data are determined with the two-dimensional method of chapter VI of Ref. 6, without taking account of the corrections for three-dimensional effects that are given in chapter VII of Ref. 6. It is felt that these corrections are not sufficiently well supported by experiments. Moreover, since the blades in the test compressor can be set at different angles the twist of the profiles along the blade height is more important than the stagger angle per se.

The camber angle $\phi$ for a rotor profile is obtained from

$$\phi = \frac{\Delta\beta - i_o + \delta_o}{1 - m + n} \tag{70}$$

where

$$\Delta\beta = \beta_1 - \beta_2$$

$$i_o = (K_i)_{sh} (K_i)_t (i_o)_{10} \tag{71}$$

$$\delta_o = (K_\delta)_{sh} (K_\delta)_t (\delta_o)_{10} \tag{72}$$

$(i_o)_{10}$ = zero camber incidence angle for t/c = 0.1

$(\delta_o)_{10}$ = zero camber deviation angle for t/c = 0.1

The recommended value of the correction factors $(K_i)_{sh}$ and $(K_\delta)_{sh}$ is 1.1 for C.4 profiles. The design incidence angle i for minimum loss is

$$i = i_o + n\phi \tag{73}$$

and the deviation angle $\delta$ for these conditions is

$$\delta = \delta_o + m\phi \tag{74}$$

The quantities $(i_o)_{10}$, $(\delta_o)_{10}$, m, and n are functions of the inlet flow angle $\beta_1$ and the blade solidity $\sigma$. The correction factor $(K_i)_t$ and $(K_\delta)_t$ depend on the thickness ratio t/c only. The blade stagger angle $\gamma$ of Fig. 14 is equal to

$$\gamma = \beta_1 - i - \frac{\phi}{2} \tag{75}$$

The stator blade profiles are obtained with Eqs. 70 to 74 also if $\beta_1$ is replaced by $\alpha_2$, and $\Delta\beta$ by $\Delta\alpha = \alpha_2 - \alpha_1$. The blade stagger angle is then

$$\gamma = \alpha_2 - i - \frac{\phi}{2} \tag{76}$$

For particular conditions the method of Ref. 6 gives excessively large negative incidence angles. Although negative incidence angles are beneficial for good stall margins, they may cause increased losses at the design point because of separations on the pressure side near the leading edge, especially if the latter has a small radius. If the above-mentioned situation occurs, reduced negative incidence angle $i'$ will be assumed. Reference 6 shows that for these conditions the corresponding deviation angle $\delta$ is obtained from

$$\delta' = \delta + (i' - i) \left(\frac{d\delta}{di}\right) \tag{77}$$

where the function $(d\delta/di)$ depends on solidity and inlet flow angle. For a stator blade profile, for instance, there is

$$\Delta\alpha = \phi + i - \delta = \phi' + i' - \delta'$$

where the first expression on the right-hand side holds for the design conditions obtained with the usual approach, whereas the second holds for an assumed incidence angle $i'$ from which the necessary blade camber angle $\phi'$ can be determined. With Eq. 77

$$\phi' = \Delta\alpha - i' + \delta' = \Delta\alpha - i' + \delta + (i' - i) \left(\frac{d\delta}{di}\right) \tag{78}$$

For this modified camber, the blade stagger angle $\gamma'$ of a stator is $\gamma' = \alpha_2 - i' - \frac{\phi'}{2}$ (79)

The axial distances between the blade rows of the compressor are 2.875 inches. The axial clearance between the rows must be about 0.5 in. to provide room for flow survey probes, so that the axial blade widths must be less than about 2.4 inches. Further, since each rotor has 30 and each stator 32 blades, the solidites of the rotor and the stator cascades must remain within certain limits.

The diffusion factors D and the equivalent diffusion ratios $D_{EQ}$ of Table VII are measures for the aerodynamic loading of the blade profiles in a cascade. Excessive loading is associated with flow separations, increased losses, and reduced efficiencies. At low blade loadings the efficiency of the cascade is decreased also because of large boundary layer losses. Optimum efficiencies of a row of blades are obtained if at all radii the blade profiles have the highest possible loading and the same margin of safety against stalling. The choice of the latter depends on the operating characteristics of the system for which the compressor is used.

Table VII shows that this condition is not realized in symmetrical bladings with blades of constant chord. The diffusion factor of the rotor is highest at the outer radius and very much below permissible limits at the hub radius. The opposite trend would give a better performance since it is known that for the same diffusion factor the losses are higher at the rotor tip than at the hub. The data for the stator in Table VII show that the profiles are lightly loaded at the outer radius and have increased loading at the hub radius. For stators with radial clearance gaps at the hub radius the loading should be reversed also to obtain optinum performance,since the stator losses near the hub radius are larger than those at other radii even if the diffusion factor were constant everywhere along the blade.

Within the limitations imposed by the rotor and stator blade numbers and the necessity of maintaining sufficiently large axial blade clearances for the arrangement of flow survey probes, the blade chords of rotor and stator will be varied along the radius to slightly improve the distributions of the diffusion factors of Table VII. The chosen chords for the rotor blades are given in Table VIII, those for the stator blades in Table IX. From Table VIII it can be seen that, whereas for constant chord the factor $D_R$ for the rotor changed from 0.2062 to 0.4376 from hub to tip, it now has values of 0.2498 and 0.4274 at these respective stations. The stator solidities obtained with the chosen chords are generally lower than those for constant chord in Table VII, which gave variations of $D_S$ from 0.4107 to 0.3326 from hub to tip. By Table IX these respective values are 0.4240 and 0.3762 for the stator blades with varying chord. These data show that with the symmetrical blading of Fig. 3 the earlier-mentioned optimum blade loadings cannot be achieved by varying the blade chord. Symmetrical bladings produce favorable conditions as far as the uniformity of the inlet flow velocities along the radius is concerned. Table VII shows for instance that the relative rotor inlet velocity $W_1$ decreases from 100 percent at the hub to 95.5 percent at the tip. The stator inlet velocity $V_2$ decrease in radial direction also, namely, from 100 percent at the hub to 81 percent at the outer radius. The actual magnitudes of $W_1$ and $V_2$ are nearly equal. Hence, in contrast to other blading types, symmetrical bladings are not Mach number limited by the conditions at the outer radius. For a given maximum Mach number, they can operate at higher peripheral speeds than other bladings and are therefore capable of producing a higher pressure rise per stage.

The best design of a blading would however be one that has uniform and equal velocities $W_1$ and $V_2$ along the radius, which are small with respect to the peripheral speed, and where the diffusion factors for all profiles are as high as the necessary stall margins permit. Investigations whether such bladings are possible will be carried out with a new computer program that is based on the calculating approach of this report, but with the additional refinement that the effect of the different losses along the radius will be taken into account.

The profile thicknesses of Table VIII and IX were chosen for practical and aerodynamic reasons. For the rotor the blade thickness increases about parabolically from tip to hub to obtain reduced centrifugal stresses, and the thickness of the stator blades varies about linearly to obtain small ratios t/c at the hub radius, and sufficient blade thickness at the outer radius for the attachment of the blade to its root section with the circular platform that is shown in Fig. 9 of Ref.1.

Whereas the incidence angles i of the rotor blade profiles of Table VIII seem reasonable, excessively large negative incidence angle are obtained with the design method of Ref. 6 for the stator profiles of Table IX at large radii. The data inside the heavily framed portion of Table IX are therefore replaced by those for the assumed incidence angles $i'$. The last lines in Tables VIII and IX give the axial widths of the rotor and stator blade profiles. For an axial spacing of 2.875 in.

of the stator and rotor rows, the average axial clearance between the rows is $2.875-(1_{axr} + 1_{axs})/2$. Hence this axial clearance is about 0.47 in. at the hub radius and 0.76 in. at the outer radius. These clearances are large enough for blades with the usual radial stacking line through the centers of gravity of the different profiles. It must however be examined whether for blades with swept-back leading edges, which are to be tested during the program, the blade chords of Tables VIII and IX permit to arrange inter-stage instrumentation.

The data of Tables VIII and IX will be used to establish the profile coordinates with the relations of Fig. 14. For each profile there must be determined its cross-sectional area, the coordinates of the center of gravity and the angles of the principal axes with respect to the reference line of Fig. 14, and the minimum and maximum moments of inertia. These quantities are necessary to establish the stresses and the vibratory characteristics for particular three-dimensional arrangements of the profiles in the build-up of the blades.

## 9. COMPRESSOR PERFORMANCE.

If the losses in the inlet guide vanes of the compressor are ignored, the total pressure $P_{t1}$ ahead of the first rotor at station (1) is everywhere constant. However the static pressure $p_1$ at station (1) changes along the radius, since for incompressible flows

$$p_1 = P_{t1} - \frac{\rho}{2} V_1^2 \tag{80}$$

At station (2) after the rotor the total and static pressures are denoted by $P_{t2}$ and $p_2$,
where

$$p_2 = P_{t2} - \frac{\rho}{2} V_2^2 \tag{81}$$

In contrast to prior usage in this report the region after the stator is called station (3). At this station exist the same velocities and flow angles as at station (1) but the pressures differ from those at (1), and the static and total pressures $p_3$ and $P_{t3}$ are related by

$$p_3 = P_{t_3} - \frac{\rho}{2} V_1^2 \tag{82}$$

From Eq. 7(44) of Ref. 2 the conditions along a streamline in the rotor between stations (1) and (2) can be expressed by

$$p_2 + \frac{\rho}{2} W_2^{\ 2} - \frac{\rho}{2} \omega^2 R_2^{\ 2} = p_1 + \frac{\rho}{2} W_1^{\ 2} - \frac{\rho}{2} \omega^2 R_1^{\ 2} - \Delta P_R \tag{83}$$

where $\Delta P_R$ represents the losses in the rotor. In Eq. 83 the differences in the geopotential energies of the fluis are ignored. It is customary (See Ref. 6) to express the rotor losses by

$$\Delta P_R = Y_R \frac{\rho}{2} W_1^{\ 2} \tag{84}$$

In Ref. 3 the pressure loss coefficient $Y_R$ is related to the diffusion factor $D_R$ and the rotor solidity $\sigma_R$ by

$$Y_R = \frac{2\sigma_R}{\cos\beta_2} \left[ 0.004 + 0.0639(D_R + 0.1)^{2.91} + 0.228 D_R^{\ 2.02} (1-\lambda_R)^{3.77} \right] \tag{85}$$

where

$$\lambda_R = \frac{R_{2t} - R_2}{R_{2t} - R_{2h}} = \frac{r_{2t} - r_2}{r_{2t} - r_{2h}} \tag{86}$$

The subscripts t and h refer to the outer and hub radius, respectively. Equation 85 is an approximate mathematical formulation of the empirical loss correlations of Ref. 6 which attempt to account for tip clearance effects with the factor $\lambda_R$, which increases the losses toward the rotor blade tip.

In Ref. 6 the loss in total pressure in the stator blade row is defined by

$$\Delta P_S = P_{t2} - P_{t3} = Y_S \frac{\rho}{2} V_2^{\ 2} \tag{87}$$

where by Ref. 3 the stator loss coefficient $Y_S$ can be approximated by

$$Y_S = \frac{2\sigma_S}{\cos\alpha_1}\left[0.004 + 0.0639\,(D_S + 0.1)^{2.91} + 0.057 D_S^{2.02}\,(1 - \lambda_S)^{3.77}\right] \qquad (88)$$

The quantities $\sigma_S$ and $D_S$ are the stator solidity and the stator diffusion factor,respectively, and

$$\lambda_S = \frac{R_1 - R_{1h}}{R_{1t} - R_{1h}} \qquad (89)$$

Due to the ratio $\lambda_S$ the loss coefficients $Y_S$ of Eq. 88 increase toward the hub radius where the stator blades have a radial clearance gap. Evidently Eqs. 84 and 88 do not take proper account of the tip clearance and end losses. A discussion in Section 13.7 of Ref. 2 shows that these losses must depend on the blade loading, the ratio of tip clearance and blade height, and the ratio of blade spacing and blade height, in addition to solidity. The present research program endeavors to establish a better and more physically correct evaluation of the end losses and tries to investigate whether peculiar blade shapes can be used to minimise their detrimental effects on stage performance. From Fig. 3

$$W_1^2 = (\omega R_1 - V_{u1})^2 + V_{a1}^2 = \omega^2 R_1^2 - 2\omega R_1 V_{u1} + V_1^2$$

$$W_2^2 = (\omega R_2 - V_{u2})^2 + V_{a2}^2 = \omega^2 R_2^2 - 2\omega R_2 V_{u2} + V_2^2$$

Introduced in Eq. 83, and with Eq. 84,

$$p_2 + \frac{\rho}{2} V_2^2 = p_1 + \frac{\rho}{2} V_1^2 + \rho\omega(R_2 V_{u2} - R_1 V_{u1}) - Y_R \frac{\rho}{2} W_1^2$$

With Eqs. 39, 40, 80, and 81

$$P_{t2} - P_{t1} = \rho\,\omega^2 R_m^2\, X - Y_R \frac{\rho}{2} W_1^2 \qquad (90)$$

where X is a constant, equal to 0.36578, for the bladings under consideration. With Eq. 64 the above relations, rewritten, gives

$$\Pi_{t2} = \frac{P_{t2} - P_{t1}}{\rho\omega^2 \; R_m^2} = X - \frac{Y_R}{2} (W_1^*)^2 \tag{91}$$

From Eq. 87, with Eq. 65

$$\frac{P_{t2} - P_{t3}}{\rho\omega^2 \; R_m^2} = \frac{Y_S}{2} (V_2^*)^2 \tag{92}$$

and

$$\Pi_{t3} = \frac{P_{t3} - P_{t1}}{\rho\omega^2 \; R_m^2} = X - \frac{Y_R}{2} (W_1^*)^2 - \frac{Y_S}{2} (V_2^*)^2 \tag{93}$$

For frictionless conditions the coefficients $Y_R$ and $Y_S$ would be zero and the theoretical total pressure rise in the stage would be $X\rho\omega^2 Rm^2$ by Eq. 93. Hence the total-to-total stage efficiency becomes

$$\eta_t = 1 - \frac{Y_R(W_1^*)^2 + Y_S(V_2^*)^2}{2X} \tag{94}$$

Equation 94 should actually be evaluated along particular stream surfaces; that is, $W_1^*$ and $V_2^*$ should be taken at the corresponding radii $R_1$ and $R_2$ of a stream surface. However, because of the small radial shift of the flow paths in the stage, and for the other reasons explained in paragraph 8, Eq. 94 will be determined for cylindrical stream surfaces and constant radii $R = R_1 = R_2$. A volume flow averaged stage efficiency $\overline{\eta_t}$ can be evaluated from the different efficiencies

$\eta_t$ along the radius by

$$\bar{\eta}_t = \frac{\int_{r_{1h}}^{r_{1t}} dQ_1 \, \eta_t}{\int_{r_{1h}}^{r_{1t}} dQ_1} \tag{95}$$

With Eqs. 49 and 50, with $r_{1h} = R_{1h}/R_m$, $r_{1t} = R_{1t}/R_m$,

$$\bar{\eta}_t = \frac{\int_{r_{1h}}^{r_{1t}} r_1 V_{a1}^{*} \eta_t \, dr_1}{Q_{1max}^{*}} \tag{96}$$

where from Table V, $Q_{1\,max}^{*} = 0.397007$. The average total pressure $\bar{P}_{t3}$ at station 3 is then obtained from

$$\bar{\Pi}_{t3} = \frac{\bar{P}_{t3} - P_{t1}}{\rho\omega^2 \; R_m^{\;2}} = \bar{\eta}_t \; X \tag{97}$$

In addition to the changes of the total pressures $P_{t2}$ and $P_{t3}$ in radial direction, the distributions of the static pressures $p_1$, $p_2$, and $p_3$ are of interest also for comparisons with the measured pressures and for the determination of the aerodynamic blade forces. From Eqs. 80 and 63

$$\Pi_1 = \frac{p_1 - P_{t1}}{\rho\omega^2 \; R_m^{\;2}} = -\frac{1}{2} (V_1^{*})^2 \tag{98}$$

From Eqs. 81, 91, and 65

$$\Pi_2 = \frac{P_2 - P_{t1}}{\rho\omega^2 R_m^2} = X - \frac{Y_R}{2} (W_1^*)^2 - \frac{1}{2} (V_2^*)^2 \tag{99}$$

From Eqs. 82, 93, and 63

$$\Pi_3 = \frac{P_3 - P_{t1}}{\rho\omega^2 R_m^2} = X - \frac{Y_R}{2} (W_1^*)^2 - \frac{Y_S}{2}(V_2^*)^2 - \frac{1}{2}(V_1^*)^2 \tag{100}$$

Table X shows the loss coefficients in rotor and stator for the solidities of Tables VIII and IX, and gives the dimensionless pressure coefficients. It can be noted that highest efficiency $\eta_t = 0.9422$ occurs at the mean radius, whereas the efficiencies at the tip and the hub are 0.8238 and 0.8857, respectively. The last line of Table X lists the integrands of Eq. 96. By trapezoidal integration the integral of Eq. 96 is 0.363035, hence the average stage efficiency is

$$\eta_t = \frac{0.363035}{0.397007} = 0.9144$$

Then, by Eq. 97, with X = 0.36578

$$\overline{\Pi}_{t3} = \frac{\overline{P}_{t3} - P_{t1}}{\rho\omega^2 R_m^2} = 0.33448$$

Figure 15 is a plot of the pressure coefficients of Table X to show the pressure changes along the radius of the stage. It can be noted that equal increases of the static pressures in rotor and stator occur at a radius ratio $r = R/R_m$ of about 1.1. At smaller radii most of the static pressure rise occurs in the stator, whereas the opposite occurs between r = 1.1 and the tip. Hence because of the resulting radial velocity distributions a symmetric blading does not have a constant degree of reaction of 50 percent.

With the established data the operating conditions of the compressor can be determined so that 135 HP are absorbed by one, two, or three stages. By Eqs. 30, 31, 40, and 50, the driving moment M for one stage is

$$M = Q_{1max} \rho_o \omega R_m^2 X = 2\pi \omega^2 R_m^5 \rho_o Q_{1max}^* X$$

where $Q_{1max}^* = 0.397007$ from Table V. Then, by Eq. 36, for 135 HP, $R_m = 1.2$ ft, and $\rho_o = 2.371(10^{-3})$ slug/ft$^3$,

$$\omega^3 = \frac{(135)(550)}{2\pi \rho_o R_m^5 Q_{1\,max}^* X} = 13.793\ (10^6)$$

or

$$\omega = 239.82 \quad \text{radians/sec}$$

and $$N = \frac{30}{\pi} \omega = 2290 \text{ rpm}$$

Then, by Eq. 50,

$$Q_{1max} = 1034 \quad \text{ft}^3/\text{sec}$$

From Eq. 97 with $X = 0.36578$ and $\overline{\eta}_t = 0.9114$

$$\overline{P}_{t3} - P_{t1} = \rho_o \omega^2 R_m^2 X \overline{\eta}_t = 62.4 \text{ lb/ft}^2 = 12.6 \text{ in. } H_2O$$

The following table gives these data if one, two, or three stages absorb a driving power of 135 HP.

| | | One Stage $Z = 1$ | Two Stages $Z = 2$ | Three Stages $Z = 3$ |
|---|---|---|---|---|
| Speed $N$ | (rpm) | 2290 | 1818 | 1588 |
| Volume Flow Rate $Q_{1max}$ | ($ft^3$/sec) | 1034 | 820 | 718 |
| Pressure Rise $Z(\overline{P}_{t3}-P_{t1})$ | (in. $H_2O$) | 12.6 | 15.9 | 18.1 |
| Rotor Tip Speed $\omega R_t$ | (ft/sec) | 359.7 | 285.5 | 249.4 |

Before deciding on a drive for all three speeds, a study will be undertaken to determine the blade and rotor stresses, and to investigate whether critical shaft speeds and bearing capacities permit trouble-free operation for all cases.

BIBLIOGRAPHY


1. Marshall, B. C. — "Effect of Blade Orientation on the Performance of an Axial Flow Compressor" Aeronautical Engineer's Thesis, Naval Postgraduate School, Sept. 1967

2. Vavra, M. H. — Aerothermodynamics and Flow in Turbo-Machines, Section 16.5, pp.454/463, John Wiley & Sons, N. Y. 1960

3. Steinke, R. J.; Crouse, J. E. — NASA TN D03959, May 1967

4. Lieblein, S. — NACA RM E 57A28, 1957

5. Howell, A. R. — "Development of the British Gas Turbine Jet Unit, Fluid Dynamics of Axial Compressors", ASME Reprint, p. 441, N. Y. 1947

6. Lieblein, S. — NASA SP-36, Chapter VI, 1965

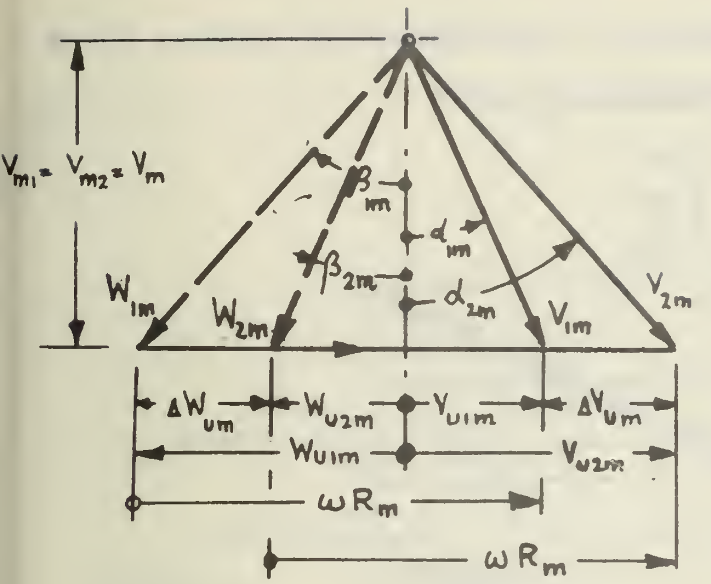


FIG. 1 VELOCITY DIAGRAM OF SYMMETRICAL STAGE AT MEAN RADIUS $R_m$

$$W_{u1m} = V_{u2m} \; ; \; W_{u2m} = V_{u1m}$$

$$\Delta W_{um} = \Delta V_{um}$$

$$\alpha_{1m} = \beta_{2m} \; ; \; \alpha_{2m} = \beta_{1m}$$

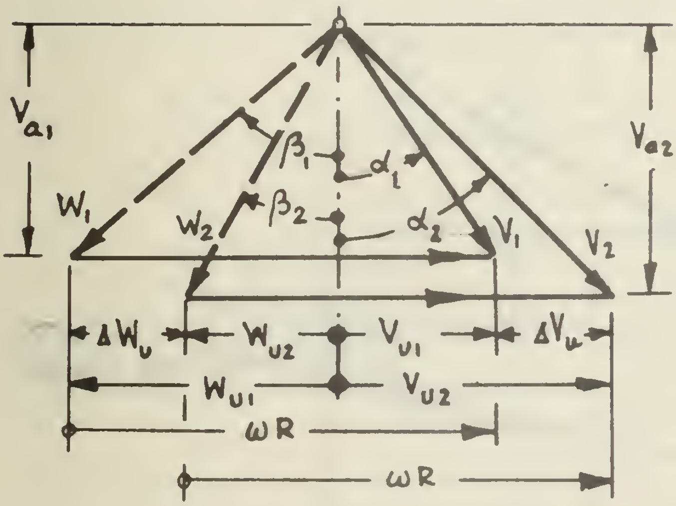


FIG. 2 VELOCITY DIAGRAM OF SYMMETRICAL STAGE FOR FLOW ON CYLINDRICAL STREAM SURFACE WITH $R_2 = R_1$

$$W_{u1} = V_{u2} \; ; \; W_{u2} = V_{u1}$$

$$\Delta W_u = \Delta V_u$$

$$\alpha_1 \neq \beta_2 \; ; \; \alpha_2 \neq \beta_1$$

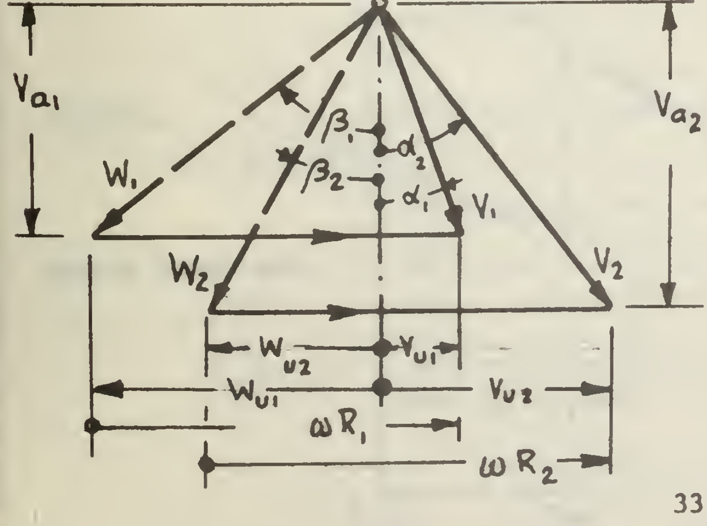


FIG. 3 VELOCITY DIAGRAM OF STAGE WITH FLOW ON ARBITRARY AXISYMMETRIC STREAM SURFACE

$$R_2 \neq R_1$$

For $R_2 V_{u2} - R_1 V_{u1} = \text{Constant} = C$

there is:

$$R_1 W_{u1} - R_2 W_{u2} = C - \omega(R_1^2 - R_2^2)$$



M.H.V. Aug 70

FIG. 4 THEORETICAL PRESSURE RISE $\Delta P_t/\eta$ IN COMPRESSOR FOR POWER OF 135 HP

SYMMETRICAL BLADING WITH $\sigma_m$ = 1

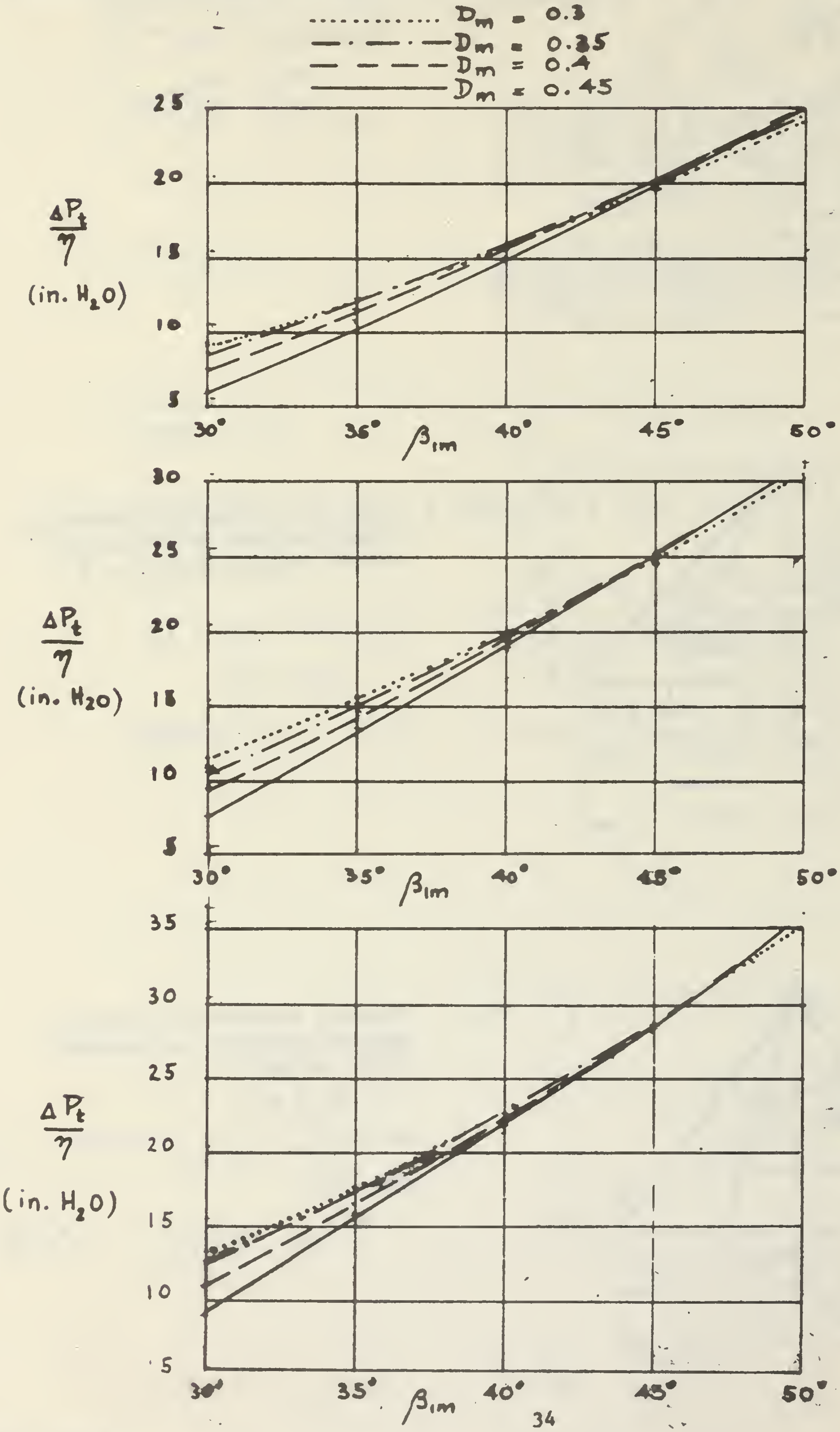


FOR ONE STAGE

FOR TWO STAGES

FOR THREE STAGES



M.H.V. Aug./7

FIG. 5 VOLUME FLOW RATE Q OF COMPRESSOR FOR POWER OF 135 HP

SYMMETRICAL BLADING WITH $\sigma_m = 1$

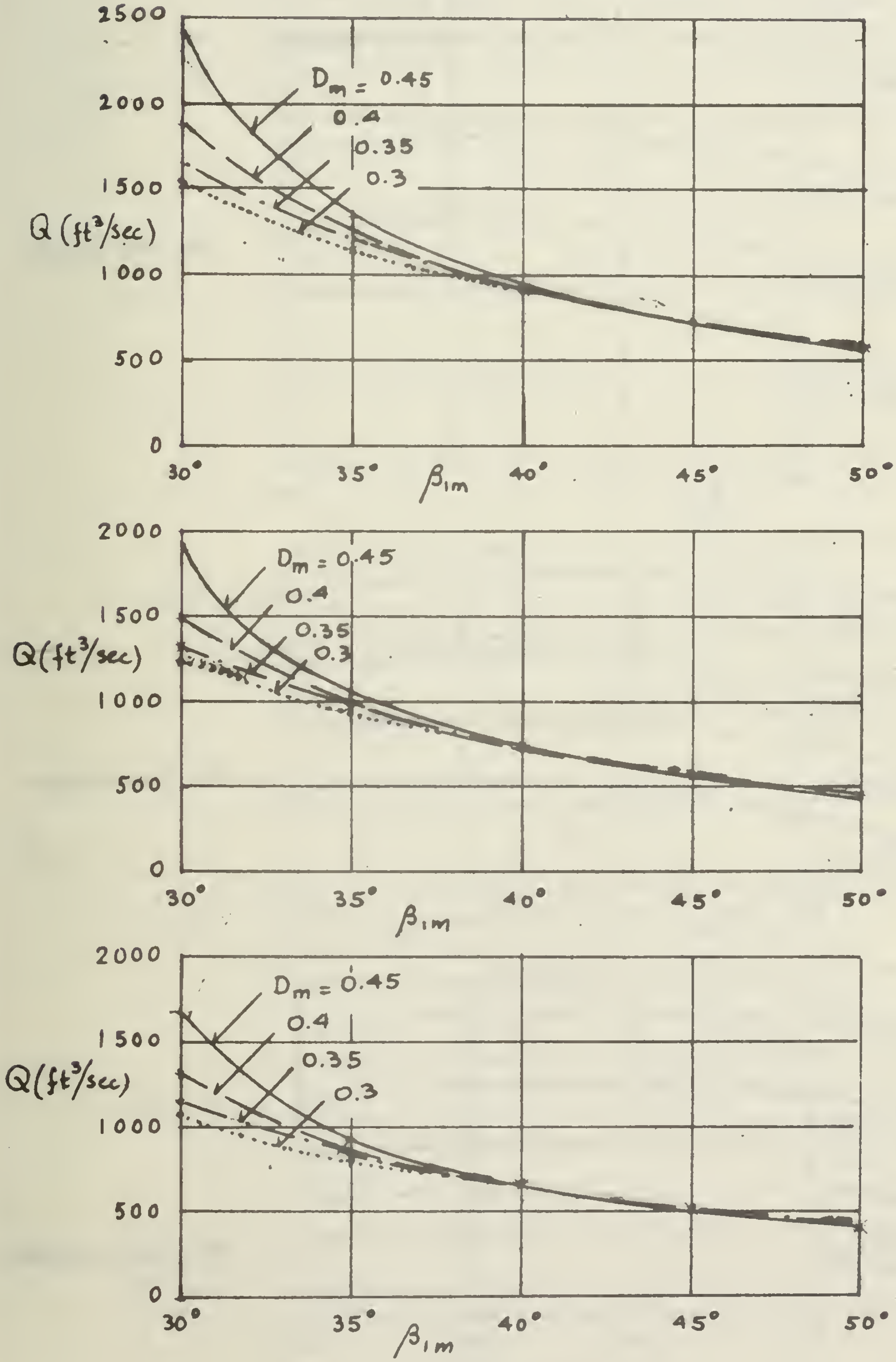


FOR ONE STAGE

FOR TWO STAGES

FOR THREE STAGES



M.H.V. Aug-70

FIG.6 SPEED OF ROTATION N OF COMPRESSOR FOR POWER OF 135 HP

SYMMETRICAL BLADING WITH $\sigma_m = 1$

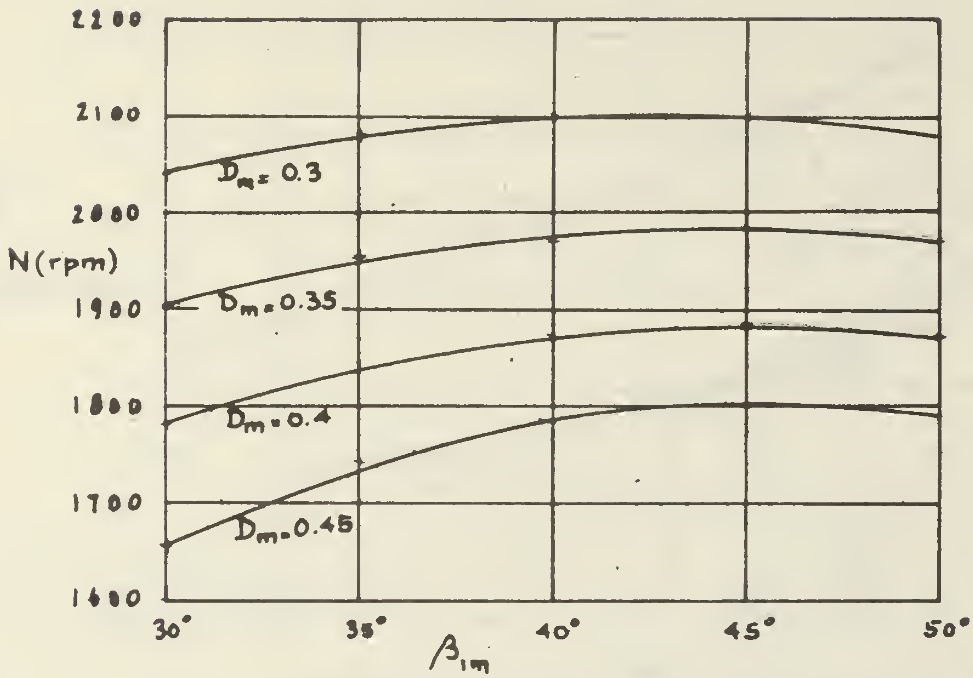


FOR ONE STAGE

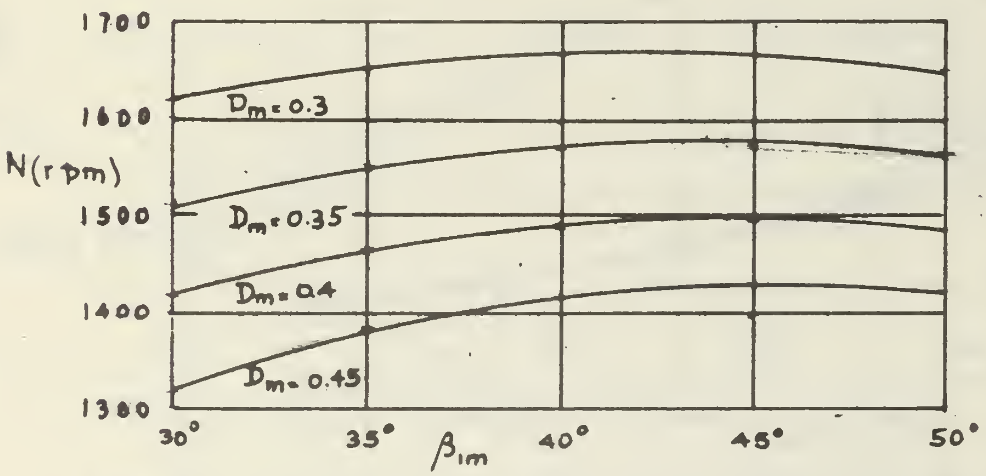


FOR TWO STAGES

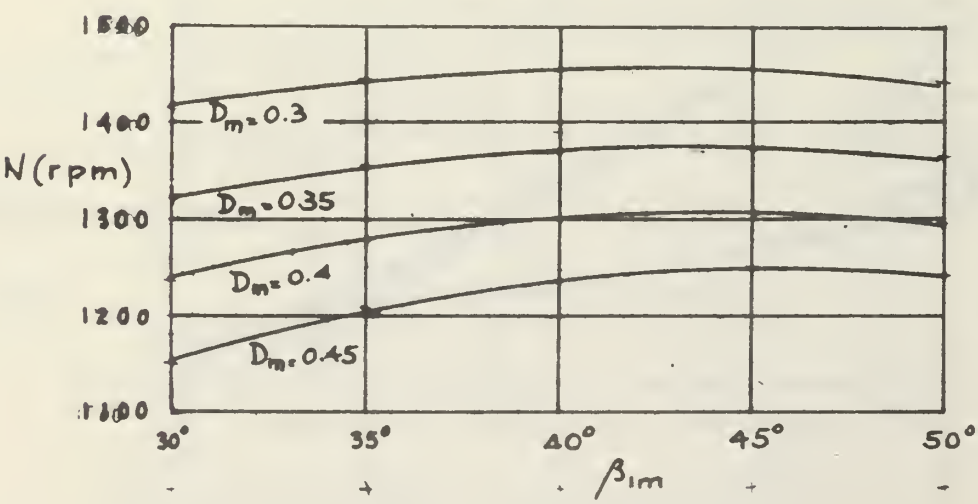


FOR THREE STAGES



M.H.Y. Aug '70

FIG. 7 FLOW DEFLECTIONS IN ROTOR CASCADE AT DIFFERENT VALUES OF FLOW INLET ANGLE $\beta_{1m}$ AND NASA DIFFUSION FACTOR $D_m$ AT BLADE SOLIDITY $\sigma_m = 1$

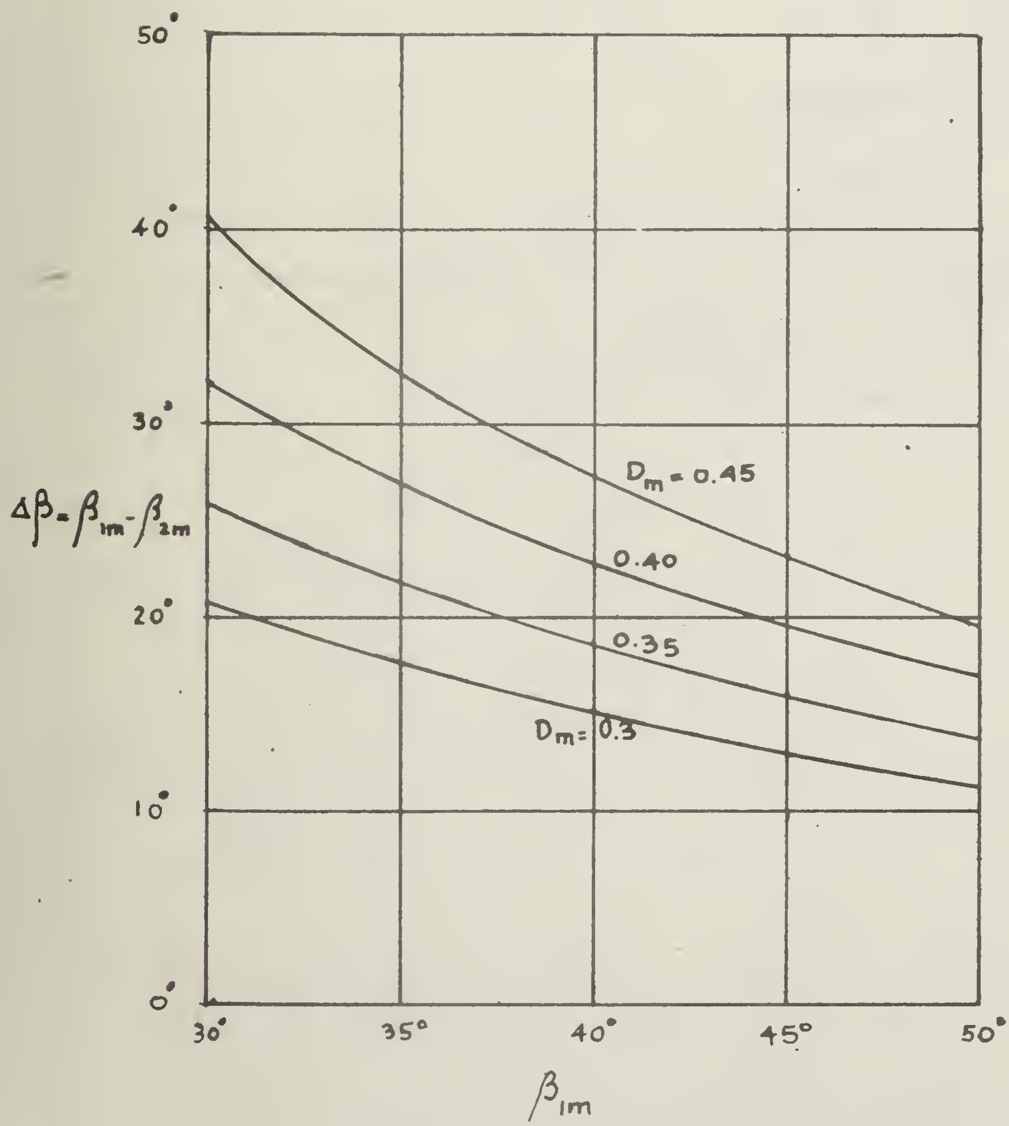




M.H.V. Aug·70

FIG. 8 DISTRIBUTION OF AXIAL VELOCITIES AHEAD AND AFTER ROTOR

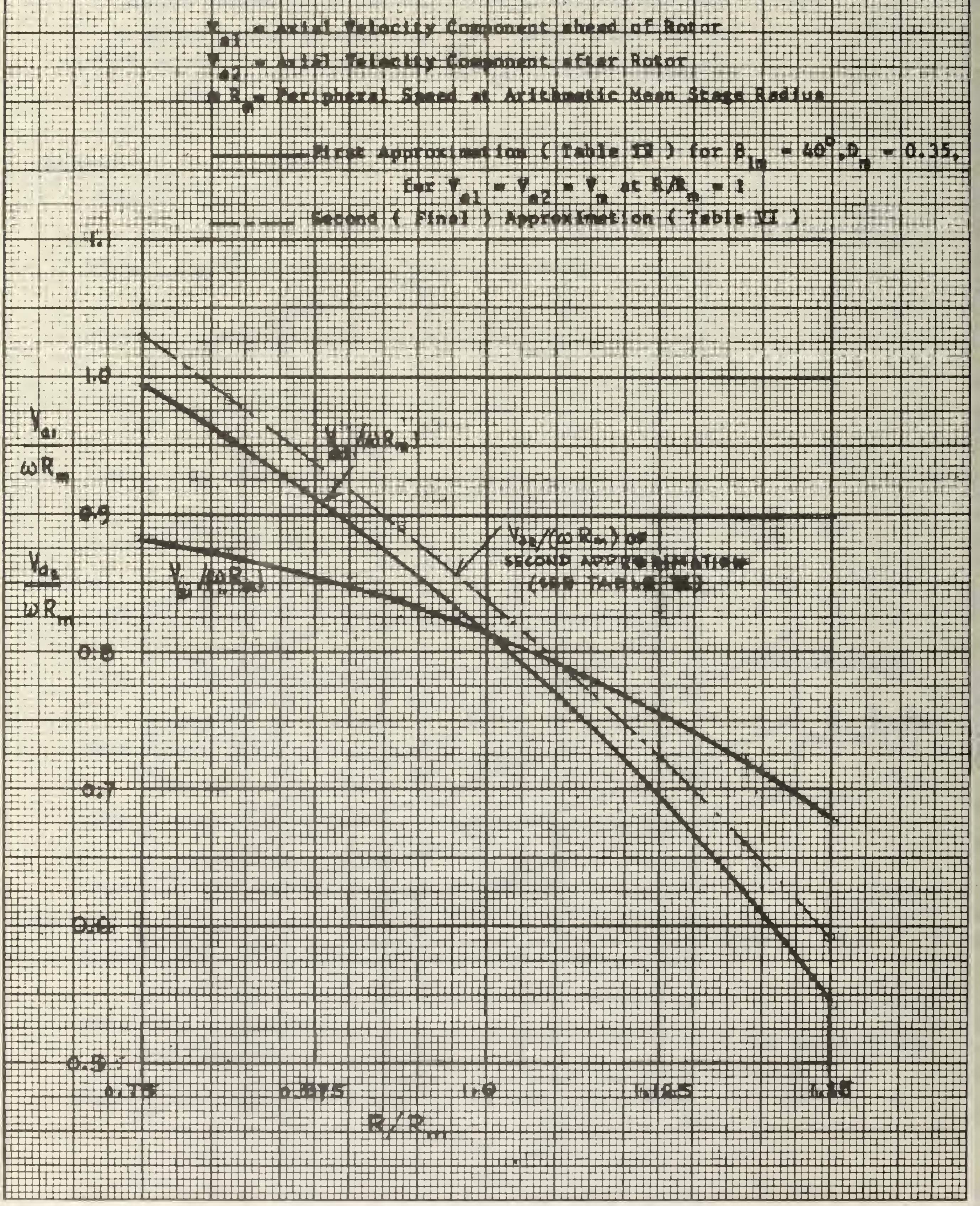




M.H.V. Aug.7

FIG. 8 RELATIVE VOLUME FLOW RATES AHEAD OF AND AFTER ROTOR OF FIRST APPROXIMATION ( SEE TABLE V )

$Q_1/Q_{1max}$ = Percentage of Total Volume Flow Rate ahead of Rotor between Radius $R_1$ and Hub Radius

$Q_2/Q_{2max}$ = Percentage of Total Volume Flow Rate after Rotor between Radius $R_2$ and Hub Radius

$R_m$ = Arithmetic Mean Stage Radius

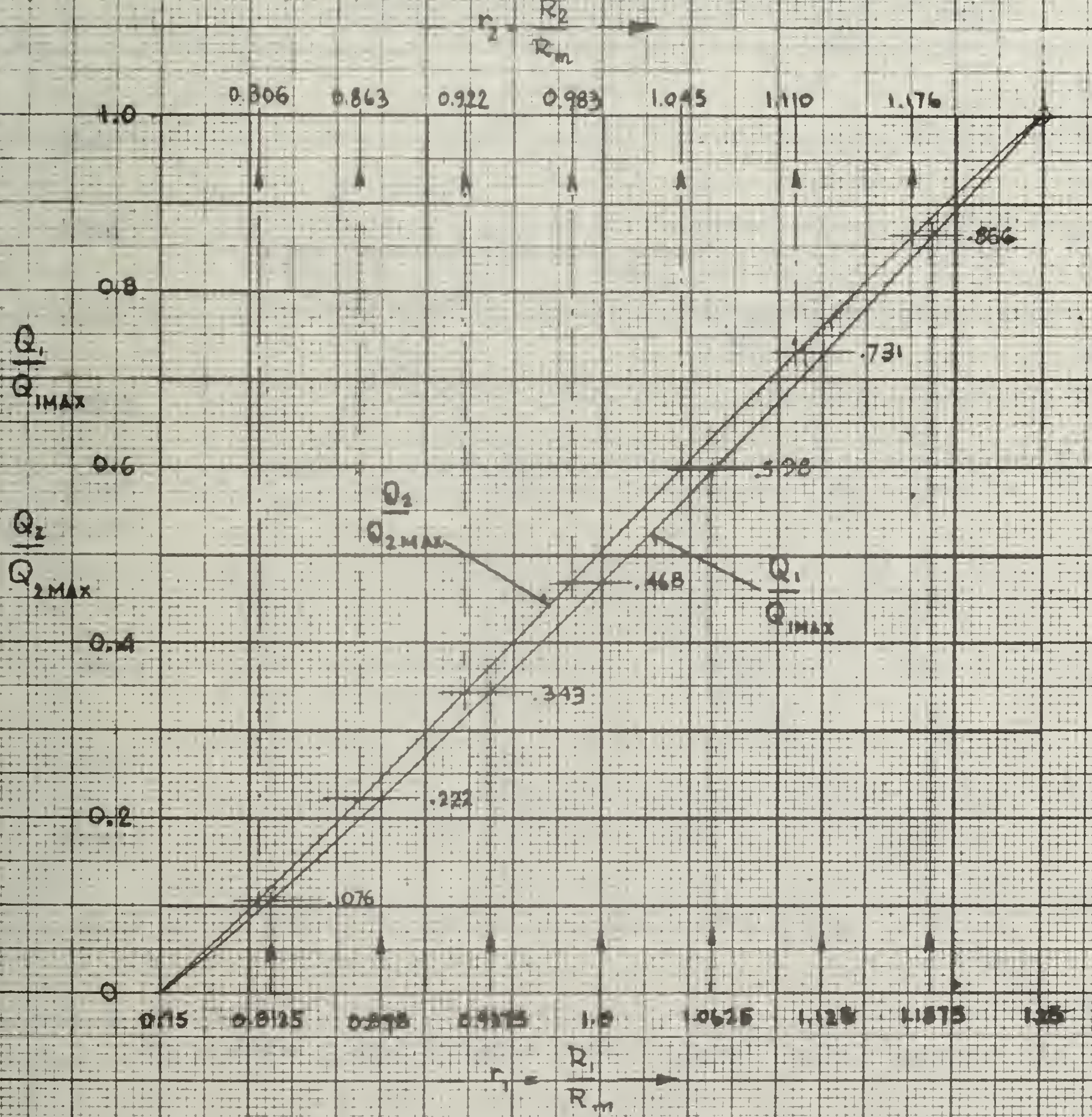




M.H.V. 8/20/70

FIG. 10 RADIAL SHIFT OF STREAM SURFACES IN ROTOR FROM DATA OF FIRST APPROXIMATION

$R_1$ - Radius of Stream Surface ahead of Rotor

$R_2$ - Radius of Stream Surface after Rotor

$R_m$ - Arithmetic Mean Stage Radius

Data Points from Fig. 9

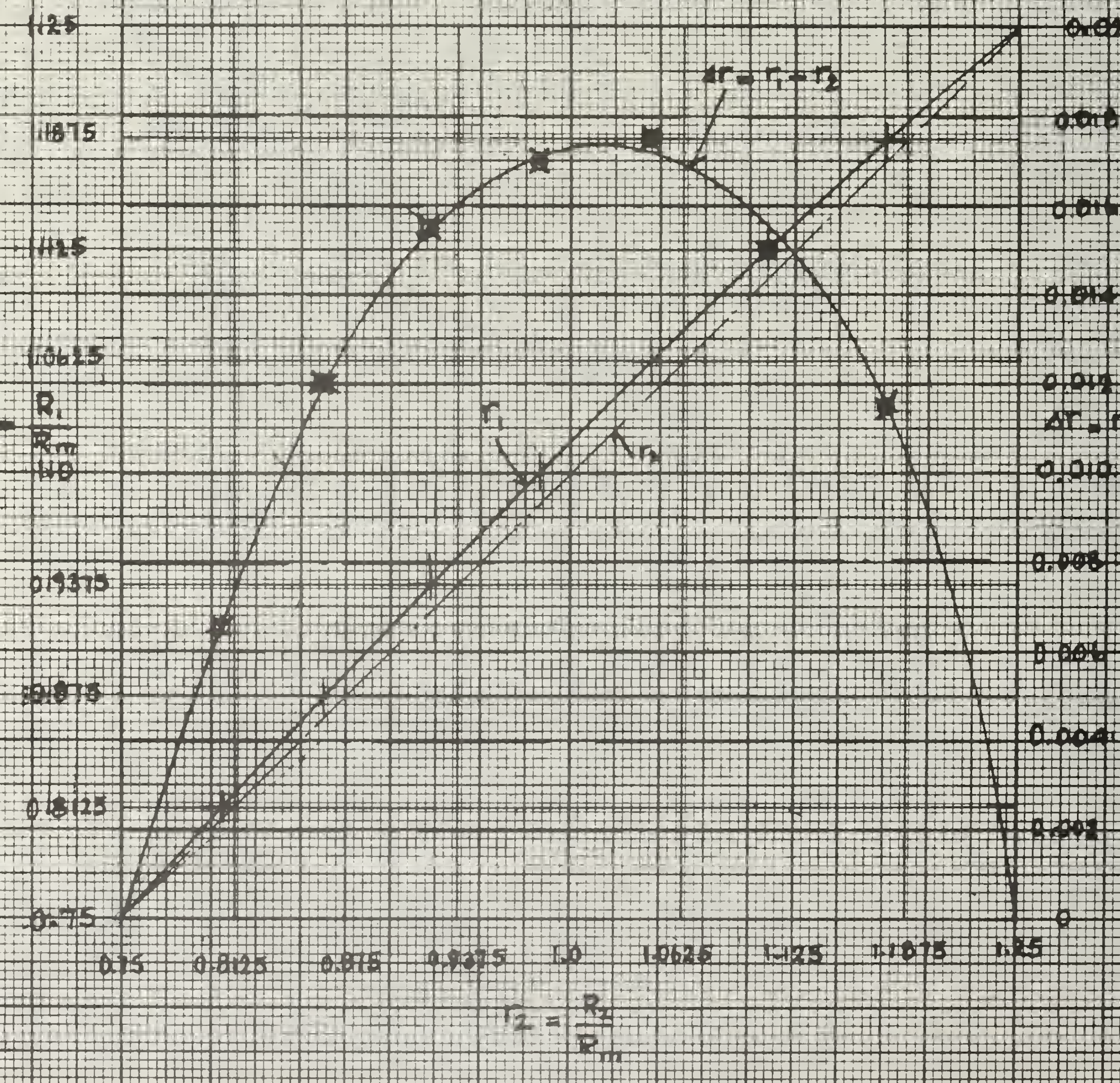

FIG.11 FUNCTION $f(r_2)$ AND $\int_1^{r_2} f(r_2)\, dr_2$ FOR SECOND APPROXIMATION

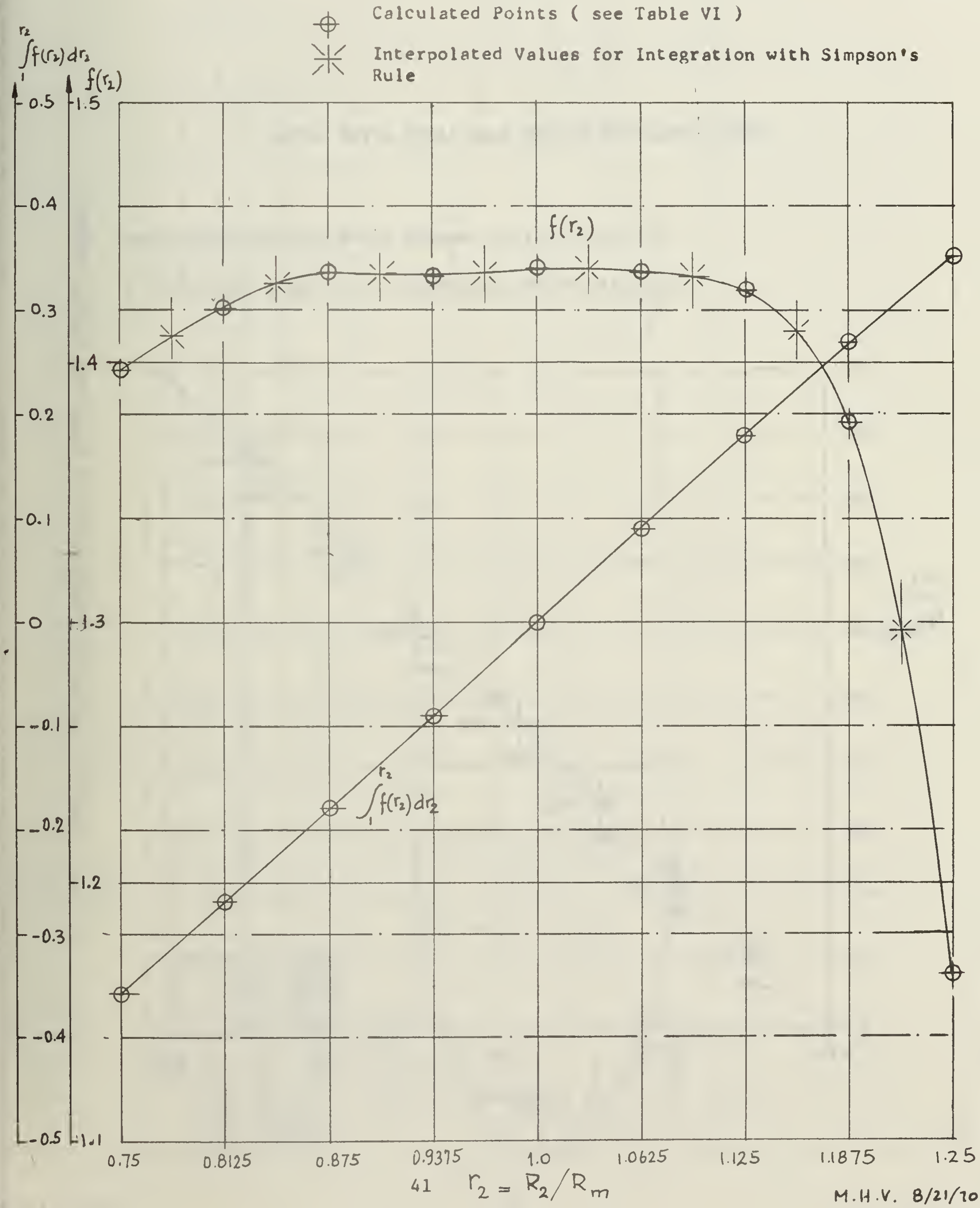

FIG.14 DETERMINATION OF PROFILE COORDINATES

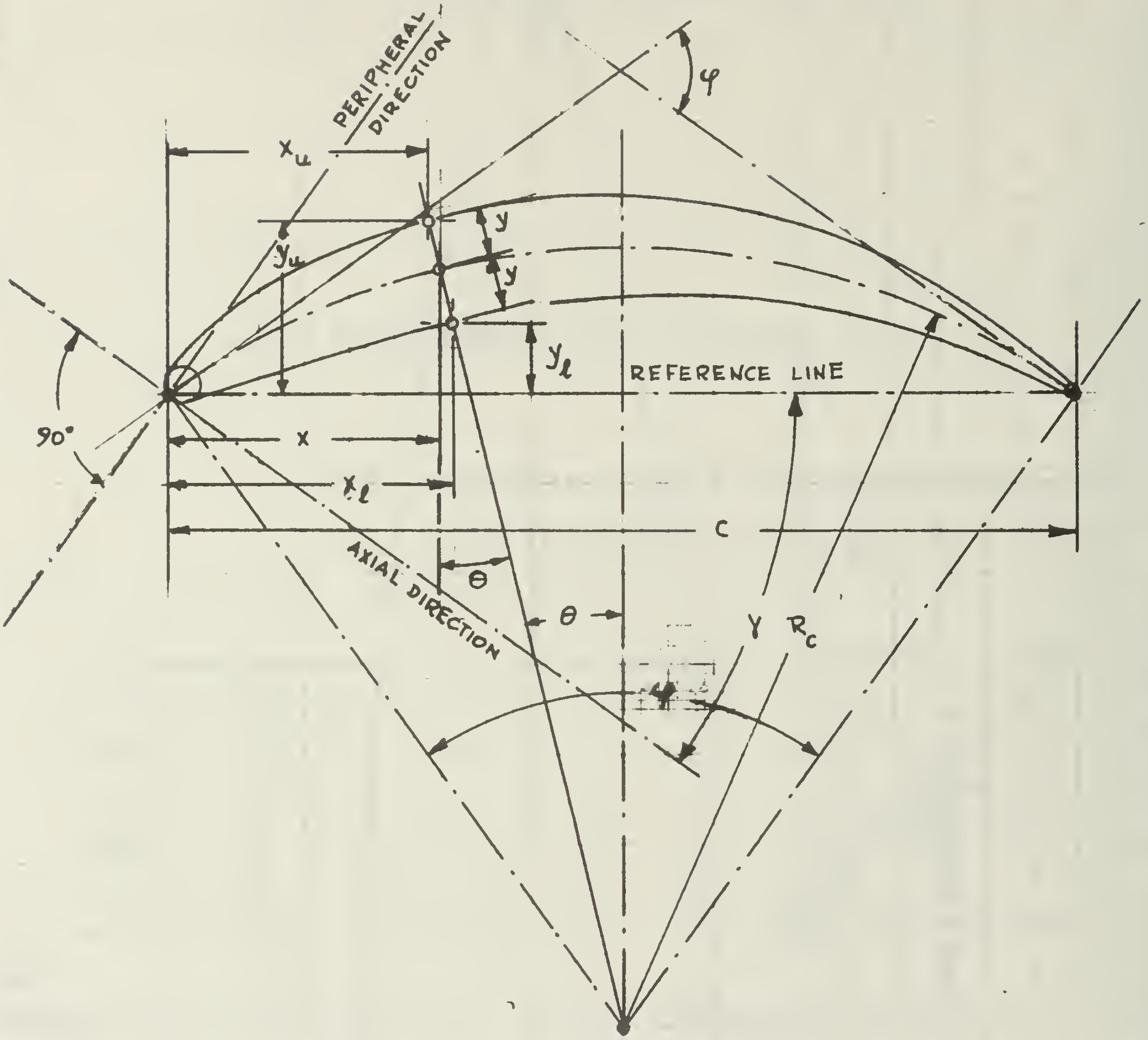


GIVEN: CHORD $c$ ; MAX. THICKNESS $t$; CAMBER ANGLE $\varphi$; STAGGER ANGLE $\gamma$

$$R_c = \frac{c}{2\sin(\varphi/2)} \; ; \qquad \sin\theta = \frac{\frac{c}{2} - x}{R_c} = \left(1 - \frac{2x}{c}\right)\sin(\varphi/2) = \left(1 - \frac{2\xi}{100}\right)\sin(\varphi/2)$$

$$\frac{x}{c} = \frac{\xi}{100} \; ; \qquad \frac{y}{c} = \frac{\eta}{100}\,\frac{t}{c}$$

$$\left.\begin{matrix} x_l \\ x_u \end{matrix}\right\} = x \pm y\sin\theta = c\,\frac{\xi}{100} \pm c\,\frac{\eta}{100}\,\frac{t}{c}\left(1 - \frac{2\xi}{100}\right)\sin(\varphi/2)$$

$$\boxed{\left.\begin{matrix} x_l/c \\ x_u/c \end{matrix}\right\} = \frac{\xi}{100} \pm \frac{\eta}{100}\,\frac{t}{c}\left(1 - \frac{2\xi}{100}\right)\sin(\varphi/2)}$$

$$\left.\begin{matrix} y_l \\ y_u \end{matrix}\right\} = R_c\left[\cos\theta - \cos(\varphi/2)\right] \mp y\cos\theta = \frac{c}{2\sin(\varphi/2)}\left[\cos\theta - \cos(\varphi/2)\right] \mp \frac{\eta}{100}\,\frac{t}{c}\,c\cos\theta$$

$$\boxed{\left.\begin{matrix} y_l/c \\ y_u/c \end{matrix}\right\} = \cos\theta\left[\frac{1}{2\sin(\varphi/2)} \mp \frac{\eta}{100}\,\frac{t}{c}\right] - \frac{1}{2}\cot(\varphi/2)}$$

M.H.V. 8/29/70

FIG.15 CALCULATED PRESSURE DISTRIBUTIONS IN STAGE (SEE TABLE X)

$P_t$ = Total Pressure , p = Static Pressure
R = Radius, ω = Angular Velocity, ρ = Mass Density
Subscripts: (1) Ahead of Rotor
(2) After Rotor,Ahead of Stator
(3) After Stator
(m) Arithmetic Mean Radius of Blading

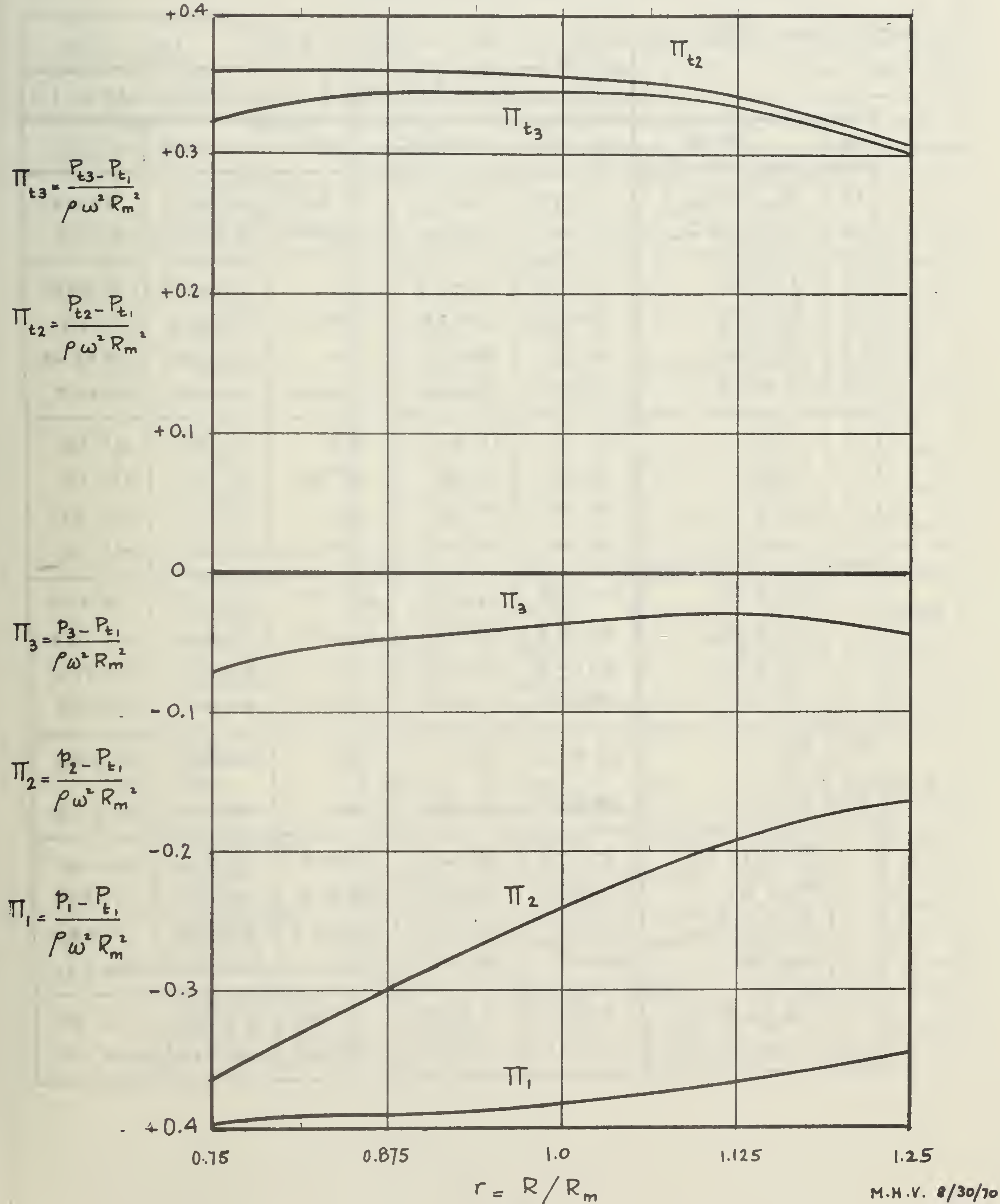

## TABLE I

THREE-DIMENSIONAL FLOW CONDITIONS IN COMPRESSOR STAGE WITH VELOCITY DIAGRAM OF FIG. 2 ON CYLINDRICAL STREAM SURFACES

| DATA AT MEAN RADIUS $R_m$: | $\beta_{1m} = 45°$ | $D_m = 0.40$ | $\sigma_m = 1.0$ |
|---|---|---|---|
| | $X = .35206$ (Eq. 4) | $Y = .45701$ (Eq. 11) | |

| Eq. | $R/R_m$ | 0.75 | 0.875 | 1.0 | 1.125 | 1.25 |
|---|---|---|---|---|---|---|
| 10 | $V_{a1}/(\omega R_m)$ | .75794 | .72607 | .67602 | .60470 | .50430 |
| 12 | $V_{a2}/(\omega R_m)$ | .88150 | .78818 | .67602 | .53173 | .31177 |
| 13 | $\tan\beta_1$ | .80443 | .87964 | 1.0 | 1.18897 | 1.51859 |
| 14 | $\tan\beta_2$ | .15915 | .29983 | .479231 | .76360 | 1.55299 |
| 16 | $\tan\alpha_2$ | .69167 | .81032 | 1.0 | 1.35213 | 2.45638 |
| 15 | $\tan\alpha_1$ | .18509 | .32548 | .47923 | .67223 | .96009 |
| | $\beta_1$ | 38° 49' | 41° 20' | 45° | 49° 56' | 56° 38' |
| | $\beta_2$ | 9° 03' | 16° 41' | 25° 36' | 37° 22' | 57° 13' |
| | $\alpha_2$ | 34° 40' | 39° 01' | 45° | 53° 31' | 67° 51' |
| | $\alpha_1$ | 10° 29' | 18° 02' | 25° 36' | 33° 55' | 43° 50' |
| | $\cos\beta_1$ | .77918 | .75085 | .70711 | .64367 | .54997 |
| | $\cos\beta_2$ | .98757 | .95787 | .90179 | .79478 | .54139 |
| | $\cos\alpha_2$ | .82244 | .77694 | .70711 | .59462 | .37706 |
| | $\cos\alpha_1$ | .98330 | .95090 | .90179 | .82991 | .72135 |
| 21 | $D_R$ | .26335 | .33111 | .40 | .47523 | .56395 |
| 22 | $D_S$ | .44507 | .42085 | .40 | .38204 | .36738 |
| | $W_1/(\omega R_m)$ | .97274 | .96700 | .95043 | .93946 | .91696 |
| | $W_2/W_1$ | .91761 | .85093 | .78412 | .71214 | .62802 |
| | $V_2/(\omega R_m)$ | 1.07181 | 1.01447 | .95043 | .89423 | .82684 |
| | $V_1/V_2$ | .71917 | .75267 | .78412 | .81481 | .84551 |
| | $\Delta\beta = \beta_1 - \beta_2$ | 29° 46' | 24° 39' | 19° 24' | 12° 34' | − 0° 35' |
| | $\Delta\alpha = \alpha_2 - \alpha_1$ | 24° 11' | 20° 59' | 19° 24' | 19° 36' | 24° 01' |

TABLE II

THREE-DIMENSIONAL FLOW CONDITIONS IN COMPRESSOR STAGE WITH VELOCITY DIAGRAM OF FIG.2 ON CYLINDRICAL STREAM SURFACES

| DATA AT MEAN RADIUS $R_m$ : | $\beta_{1m} = 45°$ | $D_m = 0.35$ | $\sigma_m = 1.0$ |
|---|---|---|---|
| | $X = .28783$ (Eq.4) | $Y = .41462$ (Eq. 11) | |

| Eq. | $R/R_m$ | 0.75 | 0.875 | 1.0 | 1.125 | 1.25 |
|---|---|---|---|---|---|---|
| 10 | $V_{a1}/(\omega R_m)$ | .74200 | .70240 | .64391 | .56188 | .44452 |
| 12 | $V_{a2}/(\omega R_m)$ | .84627 | .75515 | .64391 | .49790 | .26295 |
| 13 | $\tan\beta_1$ | .7640 | .85703 | 1.0 | 1.22878 | 1.66501 |
| 14 | $\tan\beta_2$ | .21638 | .36155 | .55300 | .87282 | 1.93903 |
| 16 | $\tan\alpha_2$ | .66987 | .79716 | 1.0 | 1.38667 | 2.81472 |
| 15 | $\tan\alpha_1$ | .24678 | .38870 | .55300 | .77343 | 1.14701 |
| | $\beta_1$ | 37° 23' | 40° 36' | 45° | 50° 51' | 59° 01' |
| | $\beta_2$ | 12° 12' | 19° 53' | 28° 57' | 41° 07' | 62° 43' |
| | $\alpha_2$ | 33° 49' | 38° 34' | 45° | 54° 12' | 70° 26' |
| | $\alpha_1$ | 13° 52' | 21° 15' | 28° 57' | 37° 43' | 48° 46' |
| | $\cos\beta_1$ | .79463 | .75930 | .70711 | .63121 | .51487 |
| | $\cos\beta_2$ | .97738 | .94042 | .87510 | .75339 | .45836 |
| | $\cos\alpha_2$ | .83082 | .78195 | .70711 | .58492 | .33477 |
| | $\cos\alpha_1$ | .97087 | .93206 | .87510 | .79101 | .65715 |
| 21 | $D_R$ | .22685 | .28753 | .35 | .41925 | .50222 |
| 22 | $D_S$ | .39098 | .36868 | .35 | .33459 | .32203 |
| | $W_1/(\omega R_m)$ | .93377 | .92506 | .91062 | .89016 | .86336 |
| | $W_2/W_1$ | .92727 | .86804 | .80803 | .74242 | .66447 |
| | $V_2/(\omega R_m)$ | 1.01860 | .96573 | .91062 | .85123 | .78546 |
| | $V_1/V_2$ | .75031 | .78034 | .80803 | .83448 | .86119 |
| | $\Delta\beta = \beta_1 - \beta_2$ | 25° 11' | 20° 43' | 16° 03' | 9° 44' | − 3° 42' |
| | $\Delta\alpha = \alpha_2 - \alpha_1$ | 19° 57' | 17° 19' | 16° 03' | 16° 29' | 21° 40' |



M.H.V. 8/22/70

TABLE III

THREE-DIMENSIONAL FLOW CONDITIONS IN COMPRESSOR STAGE WITH VELOCITY DIAGRAM OF FIG. 2 ON CYLINDRICAL STREAM SURFACES

| DATA AT MEAN RADIUS $R_m$ : | $\beta_{1m} = 40°$ | $D_m = 0.40$ | $\sigma_m = 1.0$ |
|---|---|---|---|
| | $X = .45911$ (Eq. 4) | $Y = .75594$ (Eq. 11) | |

| Eq. | $R/R_m$ | 0.75 | 0.875 | 1.0 | 1.125 | 1.25 |
|---|---|---|---|---|---|---|
| 10 | $V_{a_1}/(\omega R_m)$ | .91793 | .90101 | .86944 | .82292 | .75969 |
| 12 | $V_{a_2}/(\omega R_m)$ | 1.05203 | .96666 | .86944 | .75436 | .61012 |
| 13 | $\tan\beta_1$ | .74196 | .77674 | .83911 | .93150 | 1.06444 |
| 14 | $\tan\beta_2$ | .06552 | .18119 | .31106 | .47517 | .72339 |
| 16 | $\tan\alpha_2$ | .64737 | .72399 | | 1.01616 | 1.32538 |
| 15 | $\tan\alpha_1$ | .07508 | .19439 | | .43558 | .58097 |
| | $\beta_1$ | 36°35' | 37°50' | 40° | 42°58' | 46°47' |
| | $\beta_2$ | 3°45' | 10°16' | 17°16' | 25°25' | 35°53' |
| | $\alpha_2$ | 32°55' | 35°54' | | 45°28' | 52°58' |
| | $\alpha_1$ | 4°18' | 11° 0' | | 23°32' | 30°09' |
| | $\cos\beta_1$ | .80300 | .78975 | .76604 | .73172 | .68470 |
| | $\cos\beta_2$ | .99785 | .98398 | .95487 | .90322 | .81023 |
| | $\cos\alpha_2$ | .83945 | .81000 | | .70142 | .60230 |
| | $\cos\alpha_1$ | .99719 | .98165 | | .91680 | .86467 |
| 21 | $D_R$ | .27845 | .34012 | .4 | .46148 | .52821 |
| 22 | $D_S$ | .44866 | .42325 | .4 | .37884 | .35928 |
| | $W_1/(\omega R_m)$ | 1.14301 | 1.14088 | 1.13498 | 1.12464 | 1.10952 |
| | $W_2/W_1$ | .92238 | .86109 | .80224 | .74263 | .67869 |
| | $V_2/(\omega R_m)$ | 1.25324 | 1.19341 | 1.13498 | 1.07547 | 1.01298 |
| | $V_1/V_2$ | .73451 | .76910 | .80224 | .83461 | .86733 |
| | $\Delta\beta = \beta_1 - \beta_2$ | 32°50' | 27°34' | 22°44' | 17°33' | 10°54' |
| | $\Delta\alpha = \alpha_2 - \alpha_1$ | 28°37' | 24°54' | 22°44' | 21°56' | 12°49' |



M.H.V. 8/23/70

## TABLE IV

THREE-DIMENSIONAL FLOW CONDITIONS IN COMPRESSOR STAGE WITH VELOCITY DIAGRAM OF FIG. 2 ON CYLINDRICAL STREAM SURFACES

DATA AT MEAN RADIUS $R_m$: $\beta_{1m} = 40°$, $D_m = 0.35$, $\sigma_m = 1.0$

$X = .36578$ (Eq. 4) $\quad Y = .66233$ (Eq. 11)

| Eq. | $R/R_m$ | 0.75 | 0.875 | 1.0 | 1.125 | 1.25 |
|---|---|---|---|---|---|---|
| 10 | $V_{a1}/(\omega R_m)$ | .88082 | .85479 | .81383 | .75670 | .68022 |
| 12 | $V_{a2}/(\omega R_m)$ | .99313 | .91014 | .81383 | .69745 | .54722 |
| 13 | $\tan\beta_1$ | .70259 | .75635 | .83911 | .95820 | 1.13391 |
| 14 | $\tan\beta_2$ | .13205 | .25103 | .38965 | .57341 | .87476 |
| 16 | $\tan\alpha_2$ | .62312 | .71033 | .83910 | 1.03957 | 1.40948 |
| 15 | $\tan\alpha_1$ | .14889 | .23575 | .38965 | .52850 | .70372 |
| | $\beta_1$ | 35° 05' | 37° 06' | 40° | 43° 46' | 48° 35' |
| | $\beta_2$ | 7° 31' | 14° 06' | 21° 17' | 29° 50' | 41° 11' |
| | $\alpha_2$ | 31° 56' | 35° 23' | | 46° 07' | 54° 39' |
| | $\alpha_1$ | 8° 28' | 13° 16' | | 27° 51' | 35° 08' |
| | $\cos\beta_1$ | .81824 | .79756 | .76604 | .72204 | .66143 |
| | $\cos\beta_2$ | .99139 | .96990 | .93176 | .86750 | .75266 |
| | $\cos\alpha_2$ | .84871 | .81525 | | .69325 | .57863 |
| | $\cos\alpha_1$ | .98910 | .97331 | | .88412 | .81780 |
| 21 | $D_R$ | .23932 | .29511 | .35 | .40738 | .47087 |
| 22 | $D_S$ | .39528 | .37717 | .35 | .33105 | .31387 |
| | $W_1/(\omega R_m)$ | 1.07649 | 1.07175 | 1.06238 | 1.04801 | 1.02841 |
| | $W_2/W_1$ | .93056 | .87552 | .82214 | .76712 | .70695 |
| | $V_2/(\omega R_m)$ | 1.17016 | 1.11639 | 1.06238 | 1.00605 | .94571 |
| | $V_1/V_2$ | .76101 | .78665 | .82214 | .85072 | .87950 |
| | $\Delta\beta = \beta_1 - \beta_2$ | 27° 34' | 23° | 18° 43' | 13° 56' | 7° 24' |
| | $\Delta\alpha = \alpha_2 - \alpha_1$ | 23° 28' | 22° 07' | 18° 43' | 18° 16' | 19° 31' |



M.H.V. 8/24/70

TABLE V FLOW RATE CALCULATIONS FROM FIRST APPROXIMATION

| EQ | $r_1 = R_1/R_m$ , $r_2 = R_2/R_m$ | 0.75 | 0.8125 | 0.875 | 0.9375 | 1.0 | 1.0625 | 1.125 | 1.1875 | 1.25 |
|---|---|---|---|---|---|---|---|---|---|---|
| 10 | $V_{a1}^* = V_{a1}/(\omega R_m)$ | .88082 | .86965 | .85479 | .83622 | .81383 | .78743 | .75670 | .72119 | .68022 |
| 12 | $V_{a2}^* = V_{a2}/(\omega R_m)$ | .99313 | .95300 | .91014 | .86399 | .81383 | .75875 | .69745 | .62801 | .54722 |
| 49 | $Q_1^*$ | 0 | .042 725 | .088 179 | .136 051 | .185 982 | .237 559 | .290 307 | .343 673 | .397 007 |
| | $Q_{1\,max}^*$ | | | | | | | | | $\boxed{.397007}$ |
| | $Q_1^*/Q_{1max}^* = Q_1/Q_{1max}$ | 0 | .107 618 | .222 109 | .342 692 | .468 460 | .598 375 | .731 239 | .865 660 | 1 |
| 52 | $Q_2^*$ | 0 | .047 474 | .096 558 | .146 757 | .197 501 | .248 126 | .297 839 | .345 664 | .390 345 |
| | $Q_{2\,max}^*$ | | | | | | | | | $\boxed{.390345}$ |
| | $Q_2^*/Q_{2max}^* = Q_2/Q_{2max}$ | 0 | .121 621 | .247 366 | .375 967 | .505 965 | .635 658 | .763 015 | .885 535 | 1 |

| EQ. | $r_2 = R_2/R_m$ | | 0.75 | 0.8125 | 0.875 | 0.9375 | 1.0 | 1.0625 | 1.125 | 1.1875 | 1.25 | |
|---|---|---|---|---|---|---|---|---|---|---|---|---|
| | $r_1$ | | .75 | .8198 | .8879 | .9535 | 1.0173 | 1.0794 | 1.1399 | 1.1979 | 1.25 | |
| 55 | $\partial r_1/\partial r_2$ | | 1.129 | 1.102 | 1.072 | 1.036 | 1.008 | .980 | 0.952 | .900 | .755 | |
| 46 | $f(r_2)$ | | 1.39736 | 1.42030 | 1.43482 | 1.43293 | 1.43629 | 1.43447 | 1.42774 | 1.37672 | 1.16467 | |
| 47 | $\int_1^{r_2} f(r_2)\,dr_2$ | | -.35669 | -.26859 | -.17926 | -.08964 | 0 | .08972 | .17923 | .26726 | .35194 | |
| 47 | $V_{m2}^* = 0.844$ | $V_{a2}^*$ | 1.03404 | .99042 | .94424 | .89553 | 0.844 | .78906 | .73014 | .66714 | .60033 | |
| 52 | | $Q_2^*$ | | | | | | | | | .408091 | * |
| 47 | $V_{m2}^* = 0.8382$ | $V_{a2}^*$ | 1.02921 | .98548 | .93906 | .89006 | 0.8382 | .78285 | .72343 | .65978 | .59215 | |
| 52 | | $Q_2^*$ | | | | | | | | | .405012 | * |
| 47 | $V_{m2}^* = 0.838$ | $V_{a2}^*$ | 1.02904 | .98531 | .93888 | .88988 | 0.838 | .78264 | .72320 | .65953 | .59187 | |
| 52 | | $Q_2^*$ | 0 | .049136 | .099826 | .151569 | .203827 | .256001 | .307412 | .357312 | .404907 | * |
| | | $Q_2/Q_{2max}$ | 0 | .121350 | .246542 | .374332 | .503390 | .63225 | .75922 | .88246 | 1 | |
| 47 | $V_{m2}^* = 0.837$ | $V_{a2}^*$ | 1.02823 | .98446 | .93799 | .88893 | 0.837 | .78157 | .72204 | 65826 | .59045 | |
| 52 | | $Q_2^*$ | | | | | | | | | .404375 | * |

* Required Value for $Q_{2max}^*$ = 0.404947 to satisfy Continuity with Blockage Factor $k_B$ = 0.98

At $V_{m2}^*$ = 0.838 the Value of $Q_{2max}^*$ is 99.99% of Required Value

M.H.V. 8/25/70

TABLE VII SUMMARY OF FLOW PROPERTIES IN STAGE

| | Eq. | TABLE | $r_1 = R_1/R_m$ | 0.75 | 0.8125 | 0.875 | 0.9375 | 1.0 | 1.0625 | 1.125 | 1.1875 | 1.25 |
|---|---|---|---|---|---|---|---|---|---|---|---|---|
| ROTOR INLET | | V | $V_{a1}^* = V_{a1}/(\omega R_m)$ | .88082 | .86965 | .85479 | .83622 | .81383 | .78743 | .75670 | .72119 | .68022 |
| | 56 | | $V_{u1}^*$ | .131 147 | .181 155 | .228 483 | .273 667 | .317 110 | .359 118 | .399 931 | .439 737 | .478 688 |
| | 57 | | $W_{u1}^*$ | .618853 | .631 345 | .646 517 | .663833 | .682890 | .703 382 | .725 069 | .747 763 | .771 312 |
| | 58 | | $\tan\alpha_1$ | .148 892 | .208 308 | .267 297 | .327 267 | .389 651 | .456064 | .528 520 | .609 739 | .703 725 |
| | 59 | | $\tan\beta_1$ | .702 588 | .725 976 | .756 346 | .793849 | .839 106 | .893 262 | .958198 | 1.036845 | 1.133915 |
| | | | $\cos\alpha_1$ | .989097 | .978988 | .966 083 | .950 399 | .931764 | .909845 | .884 114 | .853803 | .817800 |
| | | | $\cos\beta_1$ | .818236 | .809 235 | .797 564 | .783213 | .766042 | .745787 | .722 037 | .694202 | .661 430 |
| | 63 | | $V_1^*$ | .890 530 | .888 318 | .884 800 | .879862 | .873 429 | .865 465 | .855 885 | .844680 | .831 770 |
| | 64 | | $W_1^*$ | 1.076 487 | 1.074 657 | 1.071 751 | 1.067 679 | 1.062 383 | 1.055837 | 1.048007 | 1.038 876 | 1.028407 |
| | Eq. | TABLE | $r_2 = R_2/R_m$ | 0.75 | 0.8125 | 0.875 | 0.9375 | 1.0 | 1.0625 | 1.125 | 1.1875 | 1.25 |
| ROTOR DISCHARGE | | VI | $r_1$ for same stream surface | .75 | .8198 | .8879 | .9535 | 1.0173 | 1.0794 | 1.1399 | 1.1979 | 1.25 |
| | | VI | $V_{a2}^* = V_{a2}/(\omega R_m)$ | 1.02904 | .98531 | .93888 | .88988 | .838 | .78264 | .72320 | .65953 | .59187 |
| | 45 | | $V_{u2}^*$ | .618853 | .638678 | .659512 | .679969 | .700340 | .720416 | .740067 | .758208 | .771312 |
| | 60 | | $W_{u2}^*$ | .131147 | .173 822 | .215488 | .257 531 | .299660 | .342084 | .384 933 | .429 292 | .478688 |
| | 61 | | $\tan\alpha_2$ | .601 389 | .648 200 | .702446 | .764113 | .835 727 | .920495 | 1.023 323 | 1.149619 | 1.303178 |
| | 62 | | $\tan\beta_2$ | .127 446 | .176 413 | .229516 | .289400 | .357590 | .437090 | .532 263 | .650 906 | .808772 |
| | | | $\cos\alpha_2$ | .856 967 | .839133 | .818291 | .794585 | .767 317 | .735750 | .698909 | .656302 | .608775 |
| | | | $\cos\beta_2$ | .991976 | .984793 | .974 658 | .960583 | .941608 | .916 295 | .882745 | .838 096 | .777530 |
| | 65 | | $V_2^*$ | 1.200793 | 1.174200 | 1.147367 | 1.119931 | 1.092 117 | 1.063731 | 1.034755 | 1.004918 | .972231 |
| | 66 | | $W_2^*$ | 1.037 363 | 1.000525 | .963292 | .926395 | .889966 | .854135 | .819263 | .786938 | .761218 |
| | | | $\Delta V_u^* = \Delta W_u^* = V_{u2}^* - V_{u1}^*$ | .487707 | .457523 | .431029 | .406302 | .383230 | .361298 | .340136 | .318471 | .292624 |
| ROTOR | | | $W_2/W_1$ | .963656 | .931018 | .898802 | .867672 | .837708 | .808965 | .781734 | .757490 | .740191 |
| | 17 | | $(D_R)_0$ | .2062 | .2419 | .2771 | .3107 | .3426 | .3728 | .4008 | .4245 | .4376 |
| | 68 | | $(D_{EQR})_0$ | 1.3284 | 1.3749 | 1.4273 | 1.4811 | 1.5352 | 1.5896 | 1.6431 | 1.6912 | 1.7205 |
| STATOR | | | $V_1/V_2$ | .74162 | .75653 | .771157 | .78564 | .79976 | .81360 | .82714 | .84055 | .85553 |
| | 18 | | $(D_S)_0$ | .4107 | .4018 | .3932 | .3844 | .3757 | .3668 | .3578 | .3476 | .3326 |
| | 69 | | $(D_{EQS})_0$ | 1.7416 | 1.708 | 1.6749 | 1.6419 | 1.6088 | 1.5750 | 1.5043 | 1.5037 | 1.4611 |

M.H.V. 8/28/70

TABLE VIII ROTOR BLADE PROFILES FOR ASSUMED CHORDS AND THICKNESSES

NUMBER OF ROTOR BLADES = 30

| EQ. | TABLE | REF. 6 FIG. | REF. 6 PAGE | $r = R/R_m$ | 0.75 | 0.8125 | 0.875 | 0.9375 | 1.0 | 1.0625 | 1.125 | 1.1875 | 1.25 |
|---|---|---|---|---|---|---|---|---|---|---|---|---|---|
| | | | | R (in.) | 10.8 | 11.7 | 12.6 | 13.5 | 14.4 | 15.3 | 16.2 | 17.1 | 18.0 |
| | | | | ASSUMED CHORD $c_R$ (in.) | 2.4 | 2.5 | 2.6 | 2.7 | 2.8 | 2.9 | 3.0 | 3.1 | 3.2 |
| | | | | SOLIDITY $\sigma_R$ | 1.061 | 1.020 | .985 | .955 | .928 | .905 | .884 | .865 | .849 |
| 17 | | | | $D_R$ | .2498 | .2777 | .3053 | .3316 | .3566 | .3801 | .4018 | .4197 | .4274 |
| 68 | | | | $D_{EQR}$ | 1.3662 | 1.4105 | 1.4567 | 1.5034 | 1.5506 | 1.5978 | 1.6442 | 1.6855 | 1.7085 |
| | | | | ASSUMED MAX. THICK. (in.) | .30 | .276 | .256 | .239 | .225 | .214 | .206 | .201 | .20 |
| | | | | $t/c_R$ = THICKN./CHORD | .125 | .1104 | .0985 | .085 | .0764 | .0738 | .0687 | .0648 | .0625 |
| | VII | | | $\beta_1$ (°) | 35.09 | 35.99 | 37.47 | 38.44 | 40.0 | 41.77 | 43.78 | 46.04 | 48.59 |
| | VII | | | $\beta_2$ (°) | 7.26 | 10.0 | 12.93 | 16.14 | 19.68 | 23.61 | 28.02 | 33.06 | 38.96 |
| | | | | $\Delta\beta = \beta_1 - \beta_2$ (°) | 27.83 | 25.99 | 24.54 | 22.30 | 20.32 | 18.16 | 15.76 | 12.98 | 9.63 |
| | | 137 | 195 | $(i_o)_{10}$ (°) | 3.00 | 2.95 | 2.90 | 2.90 | 2.95 | 3.00 | 3.05 | 3.10 | 3.20 |
| | | 142 | 199 | $(K_i)_t$ | 1.10 | 1.045 | .995 | .930 | .890 | .865 | .832 | .810 | .790 |
| | | 161 | 212 | $(\delta_o)_{10}$ (°) | .73 | .73 | .77 | .79 | .82 | .84 | .91 | .97 | 1.06 |
| | | 172 | 219 | $(K_\delta)_t$ | 1.40 | 1.145 | .975 | .80 | .70 | .67 | .615 | .575 | .55 |
| | | 168 | 217 | $m$ | .263 | .272 | .281 | .29 | .30 | .308 | .318 | .328 | .335 |
| | | 138 | 196 | $n$ | -.11 | -.117 | -.126 | -.135 | -.145 | -.155 | -.166 | -.180 | -.197 |
| 71 | | | | $i_o$ (°) | 3.63 | 3.39 | 3.17 | 2.97 | 2.89 | 2.85 | 2.79 | 2.76 | 2.78 |
| 72 | | | | $\delta_o$ (°) | 1.12 | .92 | .82 | .69 | .63 | .62 | .62 | .61 | .64 |
| 70 | | | | $\varphi$ (°) | 40.383 | 38.494 | 37.4198 | 34.817 | 32.540 | 29.665 | 26.337 | 22.012 | 16.004 |
| 70 | | | | $\varphi$ (°, ') | 40° 23' | 38°30' | 37°25' | 34° 49' | 32°32' | 29°40' | 26° 20' | 22°01' | 16°0' |
| 73 | | | | $i$ (°) | -.812 | -1.114 | -1.545 | -1.730 | -1.828 | -1.748 | -1.582 | -1.202 | -.373 |
| 74 | | | | $\delta$ (°) | 11.74 | 11.39 | 11.33 | 10.79 | 10.39 | 9.76 | 8.99 | 7.83 | 6.0 |
| 75 | | | | $\gamma$ (°) | 15.711 | 17.857 | 20.305 | 22.761 | 25.558 | 28.686 | 32.193 | 36.236 | 40.96 |
| 75 | | | | $\gamma$ (°, ') | 15° 43' | 17°51' | 20°18' | 22°46' | 25° 33' | 28°41' | 32°12' | 36°14' | 40°58' |
| | | | | $l_{axR} = c_R \cos\gamma$ (in.) | 2.310 | 2.380 | 2.438 | 2.490 | 2.526 | 2.544 | 2.538 | 2.500 | 2.416 |

M.H.V. 8/29/70

TABLE IX STATOR BLADE PROFILES FOR ASSUMED CHORDS AND THICKNESSES

NUMBER OF STATOR BLADES = 32

| EQ. | TABLE | REF. 6 FIG. | REF. 6 PAGE | $r = R/R_m$ | 0.75 | 0.8125 | 0.875 | 0.9375 | 1.0 | 1.0625 | 1.125 | 1.1875 | 1.25 |
|---|---|---|---|---|---|---|---|---|---|---|---|---|---|
| | | | | R (in.) | 10.8 | 11.7 | 12.6 | 13.5 | 14.4 | 15.3 | 16.2 | 17.1 | 18.0 |
| | | | | ASSUMED CHORD $c_s$ (in.) | 2.60 | 2.55 | 2.50 | 2.45 | 2.40 | 2.35 | 2.30 | 2.25 | 2.20 |
| | | | | SOLIDITY $\sigma_B$ | 1.226 | 1.110 | 1.010 | .924 | .849 | .782 | .723 | .670 | .622 |
| 18 | | | | $D_S$ | .4240 | .4190 | .4147 | .4106 | .4073 | .4035 | .4001 | .3959 | .3762 |
| 69 | | | | $D_{EQS}$ | 1.7612 | 1.7328 | 1.7049 | 1.6752 | 1.6459 | 1.5774 | 1.5772 | 1.5477 | 1.5044 |
| | | | | ASSUMED MAX. THICKNESS (in.) | .170 | .180 | .190 | .200 | .210 | .220 | .230 | .240 | .250 |
| | | | | $t/c_s$ = THICKN./CHORD | .065 | .070 | .076 | .082 | .087 | .094 | .100 | .107 | .114 |
| | VII | | | $\alpha_2$ (°) | 31.039 | 32.968 | 35.086 | 37.367 | 39.886 | 42.629 | 45.660 | 48.981 | 52.449 |
| | VII | | | $\alpha_1$ (°) | 8.468 | 11.767 | 14.965 | 18.122 | 21.288 | 24.516 | 27.857 | 31.372 | 35.135 |
| | | | | $\Delta\alpha = \alpha_2 - \alpha_1$ (°) | 22.571 | 21.201 | 20.121 | 19.245 | 18.598 | 18.113 | 17.803 | 17.609 | 17.364 |
| | | 137 | 195 | $(i_o)_{10}$ (°) | 3.00 | 2.90 | 2.80 | 2.75 | 2.70 | 2.64 | 2.60 | 2.55 | 2.53 |
| | | 142 | 199 | $(K_i)_t$ | .810 | .845 | .880 | .915 | .940 | .975 | 1.0 | 1.030 | 1.055 |
| | | 161 | 212 | $(\delta_o)_{10}$ (°) | .65 | .67 | .70 | .75 | .77 | .81 | .83 | .87 | .90 |
| | | 142 | 199 | $(K_\delta)_t$ | .575 | .630 | .695 | .715 | .825 | .915 | 1.0 | 1.095 | 1.20 |
| | | 168 | 217 | m | .226 | .250 | .272 | .300 | .321 | .345 | .375 | .405 | .431 |
| | | 138 | 196 | n | -.080 | -.099 | -.115 | -.133 | -.154 | -.178 | -.202 | -.231 | -.263 |
| 71 | | | | $i_o$ (°) | 2.673 | 2.695 | 2.710 | 2.768 | 2.792 | 2.831 | 2.860 | 2.889 | 2.936 |
| 72 | | | | $\delta_o$ (°) | .411 | .464 | .535 | .590 | .699 | .815 | .913 | 1.048 | 1.188 |
| 70 | | | | $\varphi$ (°) | 29.264 | 29.138 | 29.276 | 30.100 | 31.438 | 33.746 | 37.485 | 43.319 | 51.033 |
| | | | | $\varphi$ (°, ') | 29°16' | 29°08' | 29°16' | 30°06' | 31°26' | 33°45° | 37.°29' | 43°19' | 51°02' |
| 73 | | | | $i$ (°) | .332 | -.190 | -.657 | -1.235 | -2.050 | -3.176 | -4.712 | -7.118 | -10.485 |
| 74 | | | | $\delta$ (°) | 7.024 | 7.749 | 8.498 | 9.620 | 10.790 | 12.460 | 14.970 | 18.600 | 23.180 |
| 75 | | | | $\gamma$ (°) | 16.075 | 18.588 | 21.105 | 23.552 | 26.216 | 28.932 | 31.629 | 34.439 | 37.468 |
| | | | | $\gamma$ (°, ') | 16°04' | 18°35' | 21°06' | 23°33' | 26°13' | 28°56' | 31°38' | 34°26' | 37°28' |
| | | | | $i'$ (ASSUMED INCIDENCE) | | | | | | -3.0° | -4.0° | -5.0° | -6.0° |
| | | 177 | 221 | $d\delta/di$ | | | | | | .122 | .155 | .190 | .232 |
| 78 | | | | $\varphi = \varphi'$ (°) | | | | | | 33.594 | 36.908 | 41.611 | 47.584 |
| | | | | $\varphi = \varphi'$ (°, ') | | | | | | 33°36' | 36°54' | 41°37' | 47°35' |
| 79 | | | | $\gamma = \gamma'$ (°) | | | | | | 28.832 | 31.206 | 33.175 | 34.707 |
| | | | | $\gamma = \gamma'$ (°, ') | | | | | | 28°50' | 31°12' | 33°13' | 34°42' |
| | | | | $\ell_{ax\,S} = c_s \cos\gamma$ (in.) | 2.498 | 2.417 | 2.332 | 2.245 | 2.153 | 2.059 | 1.969 | 1.882 | 1.809 |

M.H.V. 8/29/70

TABLE X ROTOR AND STATOR LOSSES, PRESSURES AND STAGE EFFICIENCIES

| EQ. | TABLE | | $r = R/R_m$ | 0.75 | 0.8125 | 0.875 | 0.9375 | 1.0 | 1.0625 | 1.125 | 1.1875 | 1.25 |
|---|---|---|---|---|---|---|---|---|---|---|---|---|
| | VIII | ROTOR LOSS | $\sigma_R$ | 1.061 | 1.020 | .985 | .955 | .928 | .905 | .884 | .865 | .849 |
| | VIII | | $D_R$ | .2498 | .2777 | .3053 | .3316 | .3566 | .3801 | .4018 | .4197 | .4274 |
| | VII | | $\cos\beta_2$ | .99198 | .98479 | .97466 | .96058 | .94161 | .91629 | .88274 | .83810 | .77753 |
| 86 | | | $1-\lambda_R$ | 0 | .125 | .25 | .375 | .5 | .625 | .75 | .875 | 1.0 |
| 85 | | | $Y_R \cos\beta_2/(2\sigma_R)$ | .00527 | .00575 | .00634 | .00742 | .00951 | .01362 | .02097 | .0331 | .05082 |
| 85 | | | $Y_R$ | .01128 | .0190 | .01141 | .01475 | .01875 | .02690 | .04200 | .06876 | .11099 |
| | IX | STATOR LOSS | $\sigma_S$ | 1.226 | 1.110 | 1.010 | .924 | .849 | .782 | .723 | .670 | .622 |
| | IX | | $D_s$ | .4240 | .4190 | .4147 | .4106 | .4073 | .4035 | .4001 | .3959 | .3762 |
| | VII | | $\cos\alpha_1$ | .98910 | .97899 | .96608 | .95040 | .93176 | .90984 | .88411 | .85380 | .81780 |
| 89 | | | $1-\lambda_S$ | 1.0 | .875 | .75 | .625 | .50 | .375 | .25 | .125 | 0 |
| 88 | | | $Y_S \cos\alpha_1/(2\sigma_S)$ | .01973 | .01536 | .01256 | .01076 | .00973 | .00914 | .00885 | .00866 | .00801 |
| 88 | | | $Y_S$ | .04890 | .03484 | .02627 | .02092 | .01773 | .01571 | .01447 | .01359 | .01218 |
| | VII | STAGE PRESSURES | $W_1^*$ | 1.07649 | 1.07466 | 1.07175 | 1.06768 | 1.06238 | 1.05584 | 1.04801 | 1.03888 | 1.02841 |
| | VII | | $V_1^*$ | .89053 | .88832 | .88480 | .87986 | .87343 | .86545 | .85588 | .84468 | .83177 |
| | VII | | $V_2^*$ | 1.20079 | 1.17420 | 1.14737 | 1.11993 | 1.09218 | 1.06373 | 1.03475 | 1.00492 | .97223 |
| 91 | | | $\Pi_{t2}$ | .35924 | .35891 | .35923 | .35737 | .35520 | .35079 | .34271 | .32867 | .30709 |
| 93 | | | $\Pi_{t3}$ | .32399 | .33489 | .34193 | .34425 | .34463 | .34190 | .33497 | .32181 | .30133 |
| 98 | | | $\Pi_1$ | -.39652 | -.39000 | -.39144 | -.38708 | -.38144 | -.37451 | -.36627 | -.35674 | -.34592 |
| 99 | | | $\Pi_2$ | -.36171 | -.33046 | -.29900 | -.26975 | -.24116 | -.21498 | -.19264 | -.17625 | -.16553 |
| 100 | | | $\Pi_3$ | -.07253 | -.05514 | -.04950 | -.04282 | -.03681 | -.03261 | -.03130 | -.03493 | -.04459 |
| 94 | | EFFICIENCY | $\eta_t$ | .8857 | .9155 | .9348 | .9411 | .9422 | .9347 | .9158 | .8798 | .8238 |
| | VII | | $V_{a1}^*$ | .88082 | .86965 | .85479 | .83622 | .81383 | .78743 | .75670 | .72119 | .68022 |
| 96 | | | $r_1 V_{a1}^* \eta_t$ | .58514 | .64692 | .69918 | .73782 | .76676 | .78202 | .77958 | .75347 | .70046 |

M.H.V. 8/30/71

INITIAL DISTRIBUTION LIST

| | | No. Copies |
|---|---|---|
| 1. | Defense Documentation Center<br>Cameron Station<br>Alexandria, Virginia 22314 | 20 |
| 2. | Library<br>Naval Postgraduate School<br>Monterey, California 93940 | 2 |
| 3. | Commander, Naval Air Systems Command<br>Navy Department<br>Washington, D. C. 20360 | 1 |
| 4. | Dr. H. J. Mueller<br>Research Administrator, Code 310<br>Naval Air Systems Command<br>Navy Department<br>Washington, D. C. 20360 | 2 |
| 5. | Mr. I. Silver<br>Propulsion Administrator, Code 330<br>Naval Air Systems Command<br>Navy Department<br>Washington, D. C. 20360 | 1 |
| 6. | Mr. J. R. Patton, Jr.<br>Office of Naval Research<br>Power Program, Code 473<br>Arlington, Virginia 22217 | 1 |
| 7. | Department of Aeronautics<br>Naval Postgraduate School<br>Monterey, California 93940 | 3 |
| 8. | Dean of Research Administration<br>Code 023<br>Naval Postgraduate School<br>Monterey, California 93940 | 2 |

## DOCUMENT CONTROL DATA - R & D

*(Security classification of title, body of abstract and indexing annotation must be entered when the overall report is classified)*

| | |
|---|---|
| 1. ORIGINATING ACTIVITY (Corporate author)<br>Naval Postgraduate School<br>Monterey, California 93940 | 2a. REPORT SECURITY CLASSIFICATION<br>Unclassified<br>2b. GROUP<br>None |

3. REPORT TITLE
Aerodynamic Design of Symmetrical Blading for Three-Stage Axial Flow Compressor Test Rig

4. DESCRIPTIVE NOTES (Type of report and inclusive dates)
Technical Report 1970

5. AUTHOR(S) (First name, middle initial, last name)
Michael H. Vavra

| 6. REPORT DATE | 7a. TOTAL NO. OF PAGES | 7b. NO. OF REFS |
|---|---|---|
| 1 September 1970 | 58 | -- |

| | |
|---|---|
| 8a. CONTRACT OR GRANT NO.<br>b. PROJECT NO.<br>c. AIRTASK No. A310310A/551A/1R01003010<br>d. | 9a. ORIGINATOR'S REPORT NUMBER(S)<br>NPS57VA70091A<br>9b. OTHER REPORT NO(S) (Any other numbers that may be assigned this report) |

10. DISTRIBUTION STATEMENT
This document has been approved for public release and sale; its distribution is unlimited.

| 11. SUPPLEMENTARY NOTES | 12. SPONSORING MILITARY ACTIVITY |
|---|---|
| | Naval Air Systems Command<br>Washington, D. C. 20360 |

13. ABSTRACT

This report deals with the aerodynamic design of an axial compressor stage with symmetrical bladings for a research program to investigate tip clearance effects in the three-stage compressor of the Turbo-Propulsion Laboratory, NPS. It establishes the blading data and the stage performance with an iterative three-dimensional approach, and gives design criteria for the drive and the flow measuring device of the test unit. The calculated distributions of the flow properties in the stage will be used for future comparisons with test data.

This task was supported by: Navy Department, Naval Air Systems Command, Code 310
AIRTASK NO. A310310A/551A/1R01003010

| 14 KEY WORDS | LINK A | | LINK B | | LINK C | |
|---|---|---|---|---|---|---|
| | ROLE | WT | ROLE | WT | ROLE | WT |
| Axial Compressor Blading | | | | | | |
| Test Rig | | | | | | |
| Aerodynamic Design | | | | | | |
| Three-Dimensional | | | | | | |